Large-N pion scattering at finite temperature:
The $f_0(500)$ and chiral restoration

Santiago Cortés,[1,*] A. Gómez Nicola,[2,†] and John Morales[3,‡]

[1]*Departamento de Física, Universidad de Los Andes, 111711 Bogotá, Colombia*
[2]*Departamento de Física Teórica II, Universidad Complutense, 28040 Madrid, Spain*
[3]*Departamento de Física, Universidad Nacional de Colombia, 111321 Bogotá, Colombia*

We consider the $O(N+1)/O(N)$ nonlinear sigma model for large N as an effective theory for low-energy QCD at finite temperature T, in the chiral limit. At $T=0$ this formulation provides a good description of scattering data in the scalar channel and dynamically generates the $f_0(500)$ pole, the pole position lying within experimental determinations. Previous $T=0$ results with this model are updated using newer analysis of pion scattering data. We calculate the pion scattering amplitude at finite T and show that it exactly satisfies thermal unitarity, which had been assumed but not formally proven in previous works. We discuss the main differences with the $T=0$ result, and we show that one can define a proper renormalization scheme with $T=0$ counterterms such that the renormalized amplitude can be chosen to depend only on a few parameters. Next, we analyze the behavior of the $f_0(500)$ pole at finite T, which is consistent with chiral symmetry restoration when the scalar susceptibility is saturated by the $f_0(500)$ state, in a second-order transition scenario and in accordance with lattice and theoretical analysis.

I. INTRODUCTION

The study of hadronic properties at finite temperature T is one of the theoretical ingredients needed to understand the behavior of matter created in relativistic heavy ion collision experiments, such as those at the RHIC and LHC (ALICE). In particular, the QCD transition involving chiral symmetry restoration and deconfinement plays a crucial role, as it is clear from the many recent advances of lattice groups in the study of the phase diagram and other thermodynamical properties [1–5].

For vanishing baryon chemical potential, the QCD transition is a crossover for $2+1$ flavors with physical quark masses, the transition temperature being about $T_c \sim 150$–160 MeV. In the chiral limit (vanishing light quark masses for fixed strange mass) it is believed to become a second-order phase transition belonging to the universality class of the $O(4)$ model [6,7]. Lattice simulations also support this fact. Actually, in [3,8] it is shown that the lattice results are compatible with a $O(N)$-like restoration pattern in the chiral limit and for physical masses, by studying the scaling of different thermodynamical observables near T_c. The expected reduction in the transition temperature from the physical mass case to the chiral limit one based on those analyses is about 15%–20%, although subject to many lattice uncertainties [3].

From the theoretical side, it is important to provide solid analysis of this chiral restoration pattern based on effective theories, given the limitations of perturbative QCD at those temperature scales. A simple model realization was historically the linear sigma model (LSM) based on $O(4) \rightarrow O(3)$ spontaneous symmetry breaking [6,9,10], where the σ component of the $O(4)$ field acquires a thermal vacuum expectation value and mass, both of them vanish at the transition in the chiral limit, and $\pi - \sigma$ mesons degenerate as chiral partners. However, such a simple description is nowadays in conflict with observations: On the one hand, the $\sigma/f_0(500)$ broad resonance produced in pion-pion scattering and listed in the PDG [11] is not compatible with a particlelike state (see [12] for a recent review). On the other hand, to consistently reproduce pion data, the LSM requires working in a strong coupling regime, invalidating the perturbative description. Nevertheless, it is clear that the $\sigma/f_0(500)$ state must play an important role in chiral restoration since it shares the quantum numbers of the QCD vacuum. Chiral symmetry restoration has also been studied within QCD inspired models like the Nambu-Jona-Lasinio or Gross-Neveu ones [13–16].

A systematic and model-independent framework that takes into account the relevant light meson degrees of freedom and their interactions is chiral perturbation theory (ChPT) [17,18]. The effective ChPT Lagrangian is constructed as a derivative and mass expansion $\mathcal{L} = \mathcal{L}_{p^2} + \mathcal{L}_{p^4} + \ldots$, where p generically denotes a meson energy scale compared to the chiral scale $\Lambda_\chi \sim 1$ GeV. The lowest-order Lagrangian $\mathcal{L}_{p^2}$ is the nonlinear sigma model (NLSM). The use of energy expansions in chiral effective theories is also justified at finite temperature to describe heavy ion physics. Pions are actually the most copiously

*js.cortes125@uniandes.edu.co
†gomez@ucm.es
‡jmoralesa@unal.edu.co

produced particles after a heavy ion collision, and most of their properties from hadronization to thermal freeze-out can be reasonably described within the temperature range where these theories are applicable. Thus, the chiral restoring behavior in terms of the quark condensate is qualitatively obtained within ChPT [19,20]. Moreover, the introduction of realistic pion interactions by demanding unitarity through the inverse amplitude method (IAM) [21] extended at finite T [22,23] improves ChPT, providing a more accurate description of several effects of interest in a heavy ion environment, such as thermal resonances, transport coefficients and electromagnetic corrections [24,25]. This approach also provides a novel understanding of the role of the $\sigma/f_0(500)$ broad resonant state in chiral symmetry restoration, without having to deal with the typical LSM drawbacks. Thus, the unitarized $\pi\pi$ scattering amplitude within ChPT at finite temperature develops a $I = J = 0$ thermal pole at $s_p = [M_p(T) - i\Gamma_p(T)/2]^2$, which for $T = 0$ corresponds to the PDG state, and whose trajectory in the complex plane as T varies shows some interesting features: The sudden drop of $M_p(T)$ towards the two-pion threshold can be interpreted in terms of chiral symmetry restoration, as opposed, for instance, to the $I = J = 1$ ρ channel where the mass drop is much softer. In addition, it has recently been shown [26] that the scalar susceptibility saturated with this σ-like state, with squared mass $M_S^2 = M_p^2 - \Gamma_p^2/4$, develops a maximum near T_c compatible with lattice data, unlike the pure ChPT prediction which is monotonically increasing. Moreover, chiral partners in the scalar-pseudoscalar sector are understood through degeneration of correlators and susceptibilities [26], something which is also directly seen in lattice data [4,5]. The role of the $f_0(500)$ state for chiral restoration could become more complicated if its possible tetraquark component is also considered at finite temperature [27].

A crucial step in the unitarized approach is the condition of exact thermal unitarity for the partial waves, with a thermal space factor modified by the Bose-Einstein distribution function. This condition holds perturbatively in ChPT [22], and the unitarized amplitude is constructed by requiring thermal unitarity to all orders, based on the physical collision processes occurring in the thermal bath [23,28]. However, it is important to emphasize that thermal unitarity for the full amplitude was not formally proven in those works; in fact, that will be one of the relevant issues discussed in the present work.

Although the approaches based on effective theories in terms of the lightest mesons provide a good description of the physics involved, especially in what concerns the effect of the lightest resonances (as discussed above), a more accurate treatment near T_c would require including heavier degrees of freedom. That is, for instance, the framework of the hadron resonance gas, which describes the system through the statistical ensemble of all free states thermally available, and where corrections due to interactions and

lattice masses can also be accounted for [29,30]. Effective chiral models including explicitly vector and axial-vector resonances have also been successfully used to depict several hadron thermal properties relevant for observables such as the dilepton and photon spectra and $\rho - a_1$ mixing or degeneration at the chiral transition [31,32].

In this work, we consider an alternative approach to the thermal pion scattering amplitude, namely, the limit of a large number of Nambu-Goldstone bosons N, or in other words, a large number of light flavors with no strangeness, as treated before at $T = 0$ in [33,34]. Previous large-N analysis at $T \neq 0$ can be found in [10,35,36]. Within this framework, the lowest order chiral effective Lagrangian for low-energy QCD will be the $O(N + 1)/O(N)$ NLSM, whose corresponding symmetry breaking pattern is $O(N + 1) \to O(N)$. As we have just commented, the latter is believed to take place in chiral symmetry restoration for $N = 3$ since $O(4)$ and $O(3)$ are, respectively, isomorphic to the isospin groups $SU_L(2) \otimes SU_R(2)$ and $SU_V(2)$. This technique has the advantage of allowing for a partial resummation of the scattering amplitude preserving many physical properties such as unitarity and the dynamical generation of the $f_0(500)$ pole, which will help us to shed more light on the chiral restoring issues discussed before. We work in the chiral limit since it simplifies considerably the analysis, besides enhancing chiral-restoring effects, as explained above. At this point, it is important to remark that massless pions remain massless at finite temperature [19,20], unlike many other instances in thermal field theory where elementary massless excitations acquire mass in the thermal bath, like high-T fermions [37], gauge fields [38,39] including large-N_f analysis [40] or when electromagnetic corrections are switched on [25].

The study of the large-N approach in low-energy QCD implies a simplification of the pion dynamics [33,34] without changing essential features such as analyticity, unitarity and the low-energy behavior for pion scattering. This is fully accomplished when working in the functional formalism of the theory [33,34,41–43] so that the Lagrangian is built as $O(N + 1)/O(N) = S^N$ covariant and $O(N + 1)$ invariant (in the chiral limit). Furthermore, as we will see in detail here, this approach will allow one to consistently describe the $f_0(500)$ state through its pole in the second Riemann sheet, where the parameters of the model are fit to pion-pion scattering phase shift data. Thanks to the fact that the model is exactly unitary, we go beyond the standard perturbative ChPT description for the scattering [18,44], as a complementary description of unitarization methods such as the IAM.

An additional observation that makes this approach suitable for studying chiral restoring effects is that in order to correctly reproduce the $f_0(500)$ pole (linked to chiral restoration as mentioned before), the dominant contributions to $\pi\pi$ scattering are the loop diagrams from the leading-order chiral Lagrangian, rather than the particular

form of higher-order terms needed to renormalize the amplitude [21,45,46]. Thus, the large-N limit framework provides a resummation of the dominant loop contributions needed to maintain exact unitarity so that the scalar pole can be correctly described.

With the above motivations kept in mind, in this work we analyze elastic pion-pion scattering at finite temperature within the large-N $O(N+1)/O(N)$ model in the chiral limit. We show that at $T = 0$ one gets reasonable values for the $f_0(500)$ pole from a fit to experimental data of a two-parameter partial wave. The extension to $T \neq 0$ includes a formal discussion of the renormalizability of the model, which as expected can be carried out in terms of $T = 0$ counterterms, although with important subtleties to be taken into account. The important feature of exact unitarity is demonstrated, including thermal corrections, something that allows us to define the second-sheet pole. Having fixed the $T = 0$ pole position, its T dependence is obtained and it is shown that the results are compatible with a second-order chiral restoring phase transition, consistently with previous determinations and lattice data.

The paper is organized as follows: In Sec. II we introduce our large-N approach within the framework of the massless NLSM and work out the diagrammatic expansion for pion scattering, both at zero and at finite temperature; Sec. III is devoted to explaining the renormalization procedure, for which technical details are relegated to the Appendix. In Sec. IV we perform the analysis of the $I = J = 0$ partial wave, providing a fit to $T = 0$ data and showing that the large-N amplitude exactly satisfies unitarity at zero and finite temperature. The latter allows us to define the Riemann second-sheet pole corresponding to the $f_0(500)$ state, which we study in detail in Sec. V, paying special attention to its thermal evolution and the connection with chiral symmetry restoration. Our conclusions are presented in Sec. VI.

II. PION SCATTERING AMPLITUDE IN THE $O(N+1)/O(N)$ NLSM

A. Diagrammatics at zero temperature

In a theory with spontaneous symmetry breaking $O(N+1) \to O(N)$, the coset space where the Nambu-Goldstone bosons (NGB) are defined is the N-dimensional sphere $S^N = O(N+1)/O(N)$. In such a theory, the most general $O(N+1)$-invariant and S^N-covariant Lagrangian in the chiral limit can be obtained as a derivative expansion of the NGB modes, whose lowest order expression is given by the NLSM [33,34,43]:

$$\mathcal{L}_{\mathrm{NLSM}} = \frac{1}{2} g_{ab}(\boldsymbol{\pi}) \partial_\mu \boldsymbol{\pi}^a \partial^\mu \boldsymbol{\pi}^b, \qquad (1)$$

where $g_{ab}(\boldsymbol{\pi})$ is a metric in the S^N manifold which is parametrized in the NGB $\boldsymbol{\pi}_a$ coordinates as

$$g_{ab}(\boldsymbol{\pi}) = \delta_{ab} + \frac{1}{NF^2} \frac{\boldsymbol{\pi}_a \boldsymbol{\pi}_b}{1 - \boldsymbol{\pi}^2/NF^2}, \qquad (2)$$

with $\boldsymbol{\pi}^2 = \sum_{a=1}^{N} \boldsymbol{\pi}_a \boldsymbol{\pi}^a$.

As explained in [43], the advantage of choosing a S^N-covariant formalism is that we can easily construct $O(N+1)$-invariant Lagrangians of higher order by properly contracting indices with the g_{ab} metric. In addition, this formalism ensures the independence of the Green functions on NGB field reparametrizations, i.e., when changing coordinates in S^N. The covariance of the quantum model is guaranteed as long as we work in the dimensional regularization (DR) scheme with $D = 4 - \epsilon$ since the metric factor appearing in the NGB quantum measure $(\mathcal{D}\boldsymbol{\pi}\sqrt{g})$, with g the metric determinant, amounts to adding to the Lagrangian a term proportional to $\delta^D(0)$ [41,42,47] which vanishes in DR [48].

Although there is no need to invoke the LSM in the above construction, one can understand the NLSM as the kinetic part of the LSM when the vacuum constraint $\boldsymbol{\pi}^2 + \sigma^2 = NF^2$ is imposed, where $v = \sqrt{N}F$ is the vacuum expectation value acquired by the σ field at tree level. In that way, it is easy to understand the N-scaling of the NF^2 constant, where $F_\pi^2 = NF^2$ is the pion decay constant at this order for the usual $N = 3$ case [18].

The Lagrangian (1) provides the standard kinetic term for the NGB fields and, along with it, an infinite set of self-interaction terms with an arbitrary even number of NGB. These interactions are obtained when the metric (2) is expanded and written as a function of two field derivatives and powers of the pion field. Hence, to obtain the relevant Feynman rules for pion scattering, we can write the Lagrangian (1) as follows:

$$\mathcal{L}_{NLSM} = \frac{1}{2} \partial_\mu \boldsymbol{\pi}_a \partial^\mu \boldsymbol{\pi}^a$$
$$+ \frac{1}{8NF^2} (\partial_\mu \boldsymbol{\pi}^2)^2 \left[1 + \frac{\boldsymbol{\pi}^2}{NF^2} + \left(\frac{\boldsymbol{\pi}^2}{NF^2} \right)^2 + \cdots \right]. \qquad (3)$$

The first term in the latter expansion gives the standard kinetic Lagrangian, and the rest are the $2n$ vertices with $n \geq 2$, represented in Fig. 1. The Feynman rule in momentum space for each vertex is $\frac{(p_A + p_B) \cdot (p_C + p_D)}{(NF^2)^{n-1}} \delta_{AB} \delta_{CD} \ldots$ with A, B and C, D the isospin indices of all possible choices of four different lines in the diagram and where the dots indicate the rest of the pair contractions, i.e., all products δ_{ij} with ij the isospin indices of pairs different from AB and CD. With these rules, we proceed to calculate the $\pi^a \pi^b \to \pi^c \pi^d$ scattering that, as is customary, is parametrized as
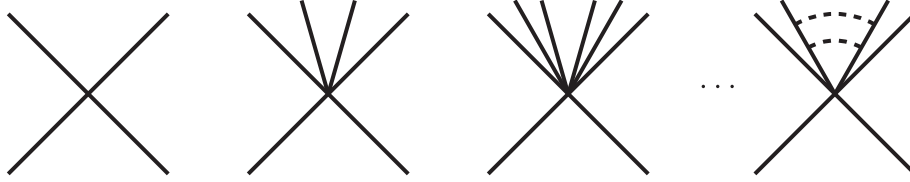
FIG. 1.   Feynman rules and diagrams at tree level, where dashed lines correspond to multiple pairs of pion lines.

$$T_{abcd}(s,t,u) = \delta_{ab}\delta_{cd}A(s,t,u) + \delta_{ac}\delta_{bd}A(t,s,u)$$
$$+ \delta_{ad}\delta_{bc}A(u,t,s). \quad (4)$$

Here, s, t, u are the Mandelstam variables $s = (p_a + p_b)^2 = (p_c + p_d)^2$, $t = (p_a - p_c)^2$, $u = (p_a - p_d)^2$, and use of isospin and crossing symmetry has been made to parametrize the amplitude. We denote $p = p_a + p_b$.

The dominant contribution to $A(s,t,u)$ in the large-N limit comes from the diagrams showed in Fig. 2. Thus, when considering diagrams of arbitrary loop order with just the four-pion vertex in Fig. 1, the dominant contribution of isospin flux is that where the pairs of lines are chosen as $(p_A + p_B) \cdot (p_C + p_D) = (q_1 + p - q_1) \cdot (q_2 + p - q_2) = s$ for an internal vertex, i.e., with no attachments to any external line (q_1 and q_2 are the four-momenta of the loops attached to that vertex) and $(p_A + p_B) \cdot (p_C + p_D) = p \cdot (q_1 + p - q_1) = s$ for the external ones. In that way, an additional factor of N is generated for every pair of vertices between a given loop, coming from a contraction $\delta_{ef}\delta^{ef} = N$, where e (f) is one of the two free indices in the first (second) vertex. The result is a net factor $s/(NF^2)$ for every vertex and an additional N for every loop, so the resulting amplitude is $\mathcal{O}(1/N)$. Other loop contributions are subdominant according to this counting.

For those vertices in Fig. 1 with more than four pions, the only way to compensate the additional $(1/N)^{n-1}$ factors of the $2n$-pion vertex is to close $2n - 4$ of them in tadpolelike contributions, giving rise to an N^{n-2} factor, so that this contribution would count the same $1/N$ as the four-pion vertex. Those tadpole insertions correspond to fields sharing the same isospin index with no derivatives since $\partial_\mu G(x)|_{x=0} = 0$, with $G(x)$ the free pion propagator. At $T = 0$, they actually vanish since the tadpole contribution $G_{T=0}(x = 0) = 0$ in the chiral limit. This will not be the case at $T \neq 0$, as we discuss in Sec. II B, and will become one of the main novelties of the present calculation. Finally, note also that in the chiral limit, the pion propagator is not

corrected by loop effects and hence needs no renormalization [42]. For instance, a tadpole correction to the self-energy would require contracting two pion lines with the same isospin index to produce an N factor, but that gives $\partial_\mu G(x)|_{x=0} = 0$, and other contributions are nondominant with respect to the tree-level propagator, which is $\mathcal{O}(1)$.

From the latter considerations, and after including the proper combinatoric factors, the $A(s,t,u)$ function in (4) depends only on s to leading order in $1/N$, which is actually one of the main simplifications of this approach, and is given by

$$A(s) = \frac{s}{NF^2}\left[1 + \frac{1}{2}\frac{1}{F^2}sJ(s) + \frac{1}{4}\frac{1}{F^4}s^2J^2(s) + \cdots\right]$$
$$= \frac{s}{NF^2}\sum_{k=0}^{\infty}\left[\frac{sJ(s)}{2F^2}\right]^k = \frac{s}{NF^2[1 - sJ(s)/2F^2]}, \quad (5)$$

where $J(s)$ is the usual logarithmically divergent loop integral which in the DR scheme reads [18]

$$J(s) = -i\int \frac{d^Dq}{(2\pi)^D}\frac{1}{q^2}\frac{1}{(p-q)^2} = J_\epsilon(\mu) + \frac{1}{16\pi^2}\ln\left(\frac{\mu^2}{-s}\right) \quad (6)$$

and $J_\epsilon(\mu)$ contains the divergent part:

$$J_\epsilon(\mu) = -2\lambda(\mu) + \frac{1}{16\pi^2}$$
$$= \frac{1}{16\pi^2}\left[\frac{2}{\epsilon} + \ln(4\pi) - \gamma + 2 - \ln\mu^2\right] + \mathcal{O}(\epsilon). \quad (7)$$

Here $\lambda(\mu) = \frac{\Gamma(1-D/2)}{2(4\pi)^{D/2}}\mu^{D-4}$, γ is Euler's constant and μ is the renormalization scale. Note that we follow the convention in [18] to define the pole contribution $\lambda(\mu)$ but we include the $1/(16\pi^2)$ contribution in the divergent part,
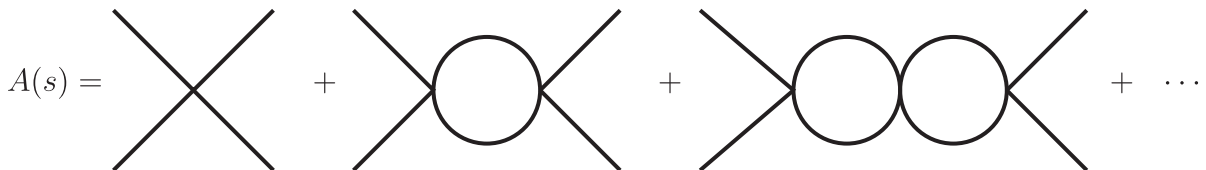

FIG. 2.   Zero-temperature scattering amplitude.

unlike in [18], in order to compare easily with previous large-N works [33,34].

We recall that for $s \in \mathbb{R}$ and $s \geq 0$ (i.e., above the two-pion threshold which in the chiral limit is at $s = 0$) we can easily obtain the imaginary parts of the loop integral as the usual unitarity cut contribution (see Sec. IV B):

$$\text{Im}J(s + i0^+) = \frac{1}{16\pi} \qquad (s > 0) \qquad (8)$$

while $\text{Im}J(s) = 0$ for $s < 0$.

In Sec. III we discuss the renormalization procedure implemented to absorb the divergent part (7), but before that, let us explain the main distinctive features of the $T \neq 0$ calculation.

B. Diagrammatics at finite temperature

We work within the imaginary-time formalism of thermal field theory [38,39] so that the thermal scattering amplitude is understood as the analytic continuation to continuous energies of the corresponding four-point Green function after performing the loop Matsubara sums and applying the LSZ standard reduction formula for $T = 0$ asymptotic states [22].

Comparing with the analysis performed in the previous section, the first observation is that the absence of renormalization for the pion propagator remains the same at $T \neq 0$, so pions do not acquire effective thermal masses, following the same diagrammatic argument as before. However, there is an important difference with the $T = 0$ case which is that the tadpole contribution is now different from zero in the chiral limit, namely [38],

$$G_T(x = 0) \equiv I_\beta = T\sum_n \int \frac{d^3\vec{q}}{(2\pi)^3} \frac{1}{\omega_n^2 + |\vec{q}|^2} = \frac{T^2}{12}, \qquad (9)$$

with the Matsubara frequencies $\omega_k = 2\pi k T$, $k \in \mathbb{Z}$.

This means that from now on, the diagrams coming from closing pairs of extra pion lines in the vertices with 6 or more legs in Fig. 1 have to be considered. To accomplish this in an efficient way, we construct the effective thermal tadpole vertex given in Fig. 3, and we rebuild the scattering amplitude to all perturbative orders with the associated Feynman rule of the thermal vertex, something that we show schematically in Fig. 4.

In addition, we have to take into account that the loop integral is also T dependent, so the thermal amplitude to leading order in $1/N$ is given by

$$A(p_0, |\vec{p}|; T) \equiv A(p; T) = \frac{s}{NF^2} \frac{f(I_\beta)}{1 - \frac{s}{2F^2} f(I_\beta) J(p_0, |\vec{p}|; T)}, \qquad (10)$$

which depends now separately on the space and time components of p due to the loss of Lorentz covariance in the thermal bath. The vertex function reads

$$f(I_\beta) = \frac{1}{1 - I_\beta/F^2}, \qquad (11)$$

and the finite-T loop integral $J(p_0, |\vec{p}|; T)$ is the analytic continuation of the external Matsubara frequency $i\omega_m \to p_0 + i0^+$ of

$$J(i\omega_m, |\vec{p}|; T)$$
$$= T\sum_n \int \frac{d^3\vec{q}}{(2\pi)^3} \frac{1}{\omega_n^2 + |\vec{q}|^2} \frac{1}{(\omega_n - \omega_m)^2 + |\vec{p} - \vec{q}|^2}, \qquad (12)$$

where $J(p_0, |\vec{p}|; T = 0) = J(s)$ in (6).

Explicit expressions for the above J integral for arbitrary three-momentum $\vec{p}$ can be found, for instance, in [25]. Its UV divergent part is the same as for $T = 0$ since Bose-Einstein factors exponentially regulate the UV behavior; therefore, we write, in general,
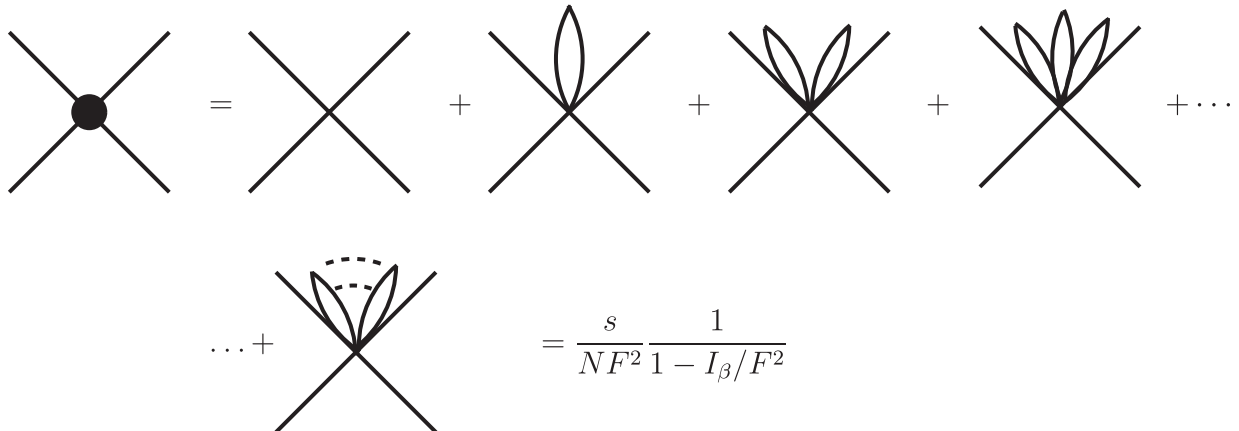

FIG. 3. Construction of the effective thermal tadpole vertex, where dashed lines correspond to multiple tadpole insertions.
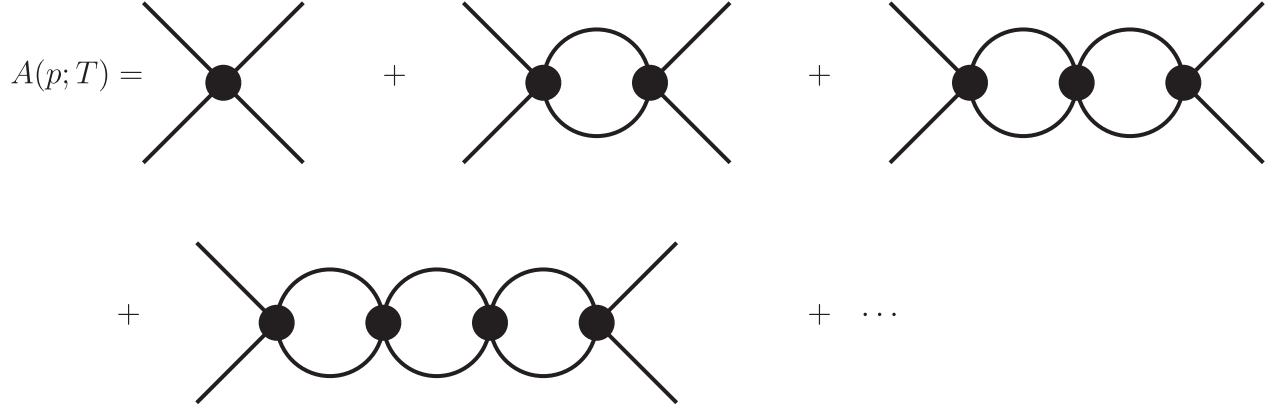
FIG. 4.   Finite-temperature scattering amplitude.

$$J(p;T) = J_\epsilon(\mu) + J_{fin}(p;T;\mu), \qquad (13)$$

with $J_\epsilon(\mu)$ in (7) and $J_{fin}(p;T;\mu)$ finite and whose scale dependence is contained only in the $T = 0$ part, namely, $J_{\text{fin}}(p;T=0;\mu) = \frac{1}{16\pi^2}\ln(-\mu^2/s)$.

In this work we are interested only in calculations in the center-of-mass (c.m.) frame (corresponding to $\vec{p} = \vec{0}$), where partial waves are defined (see Sec. IV), and moreover, we have [22]

$$J_{fin}(p_0, \vec{0}; T; \mu) = \frac{1}{16\pi^2}\ln\left(\frac{\mu^2}{-s}\right) + \delta J(s;T), \quad (14)$$

$$\delta J(s;T) = \frac{1}{\pi^2}\int_0^\infty dy \frac{y n_B(y)}{4y^2 - s}, \qquad (15)$$

where $s = p_0^2$ and $n_B(x)$ is the usual Bose-Einstein distribution function

$$n_B(x) = \frac{1}{\exp(x/T) - 1}.$$

Note that $\delta J(s;T)$ is UV finite ($y \to \infty$) thanks to the $n_B(y)$ term; besides, we can easily separate the real and imaginary parts of $\delta J(s;T)$ for $s \in \mathbb{R}$ and $s > 0$ by isolating the pole contribution at $y = \sqrt{s}/2 = |p_0|/2$ in the integrand in (15) as

$$\text{Re}\delta J(s;T) = \mathcal{P}\frac{1}{\pi^2}\int_0^\infty dy \frac{y n_B(y)}{4y^2 - s}, \qquad (16)$$

$$\text{Im}\delta J(s + i0^+;T) = \frac{1}{8\pi}n_B(\sqrt{s}/2) \qquad (s > 0), \quad (17)$$

while for $s < 0$ there is no pole in the integrand in (15).

Finally, we recall that for $s \neq 0$, $\delta J(s;T)$ is IR finite ($y \to 0^+$), while for $s \to 0^+$, it diverges as $\delta J(s;T) \sim s^{-1/2}$

so that $s\delta J(s;T)$ [as it appears in the thermal amplitude (10)] remains finite (and vanishing) in that limit.

III. RENORMALIZATION OF THE SCATTERING AMPLITUDE

We first review the main points regarding the renormalization of the model in the $T = 0$ case, as discussed in [33,34]. The scattering amplitude can be renormalized by choosing an appropriate (infinite) set of counterterm Lagrangians of higher orders in derivatives and summing their contribution to the amplitude to all orders. The philosophy behind this approach is to include only those Lagrangians needed to obtain a renormalized amplitude to leading order in $1/N$, although from the symmetry arguments explained above, many other operator structures are possible. Consistently, we can formally consider the couplings, or low-energy constants (LEC), of those additional Lagrangians to be suppressed in the $1/N$ counting. In the conventional ChPT approach [18,44] all possible terms are included to a given order in the derivative or momentum expansion, and then the LEC are fixed with experimental data, although the predictions are limited to low energies. The energy applicability range can be enlarged when additional conditions such as unitarization are implemented, and then the LEC can take, in general, different values from the perturbative ones. Here we are considering a partial resummation of the series for the amplitude, namely, the leading $1/N$ contribution, which in the end can be given in a finite form that depends only on a few parameters, to be fixed to experimental data. Nevertheless, there will be some important subtleties to be taken into account in the $T \neq 0$ case, as we will explain below, in order to ensure a renormalized amplitude with a $T = 0$ renormalization scheme. We discuss the main results in this section, while additional details are given in the Appendix.

Let us consider, for instance, the possible counterterm Lagrangians to fourth order in derivatives. It is clear that one of them satisfying the symmetry constraints would just be proportional to $\mathcal{L}^2_{\text{NLSM}}$:

$$\mathcal{L}_1 = \frac{g_1}{2NF^4} [g_{ab}(\boldsymbol{\pi}) \partial_\mu \boldsymbol{\pi}^a \partial^\mu \boldsymbol{\pi}^b]^2$$

$$= \frac{g_1}{2NF^4} \left[(\partial_\mu \boldsymbol{\pi}^a \partial^\mu \boldsymbol{\pi}_a)^2 + \mathcal{O}\left(\frac{\boldsymbol{\pi}^6}{N}\right) \right], \qquad (18)$$

where the normalization proportional to the bare coupling g_1 has been conveniently chosen. At this order there is another term allowed, i.e., $\mathcal{L}_1' \sim [g_{ab}(\boldsymbol{\pi}) \partial_\mu \boldsymbol{\pi}^a \partial_\nu \boldsymbol{\pi}^b] \times [g_{cd}(\boldsymbol{\pi}) \partial^\mu \boldsymbol{\pi}^c \partial^\nu \boldsymbol{\pi}^d]$. The LEC multiplying the two allowed terms are the counterparts of the l_1, l_2 constants of ChPT [18].

The main result at $T = 0$ is that the scattering amplitude can be rendered finite by a set of infinite counterterm Lagrangians which to $\mathcal{O}(\boldsymbol{\pi}^4)$ have the form [33]

$$\mathcal{L}_k = (-1)^{k+1} 2^{k-2} \frac{g_k}{NF^{2(k+1)}} \left[\partial_{\mu_1} \partial_{\mu_2} \cdots \partial_{\mu_k} \boldsymbol{\pi}^a \partial^{\mu_1} \partial^{\mu_2} \right.$$

$$\left. \cdots \partial^{\mu_k} \boldsymbol{\pi}_a \partial^\nu \boldsymbol{\pi}^b \partial_\nu \boldsymbol{\pi}_b + \mathcal{O}\left(\frac{\boldsymbol{\pi}^6}{N}\right) \right]. \qquad (19)$$

This reduces to (18) for $k = 1$. It is indeed always possible to find at each order an adequate contraction with the g_{ab} metric that gives rise to the terms (19), for instance, $g_{ab}(\boldsymbol{\pi}) g_{cd}(\boldsymbol{\pi}) \partial_{\mu_1} \partial_{\mu_2} \cdots \partial_{\mu_k} \boldsymbol{\pi}^a \partial^{\mu_1} \partial^{\mu_2} \cdots \partial^{\mu_k} \boldsymbol{\pi}^b \partial^\nu \boldsymbol{\pi}^c \partial_\nu \boldsymbol{\pi}^d$. Consistently, the LEC multiplying other possible terms such as $\mathcal{L}_1'$ can be considered formally suppressed in the $1/N$ counting.

The dominant contributions of the new terms to the amplitude in the $1/N$ counting arise from all possible g_k insertions in diagrams of the form shown in Fig. 5. It is actually not difficult to see that with the covariant structures discussed above, the $\mathcal{O}(\boldsymbol{\pi}^6)$ terms and higher in (19) give subdominant contributions, which also holds at $T \neq 0$. As it is explained in the Appendix, each Lagrangian (19) insertion produces a s^{k+1} power in the vertex at $T = 0$. Thus, summing up all the possible g_k insertions in the dominant loop diagrams in Fig. 5 is equivalent to the following redefinition of the four-pion vertex [33]:
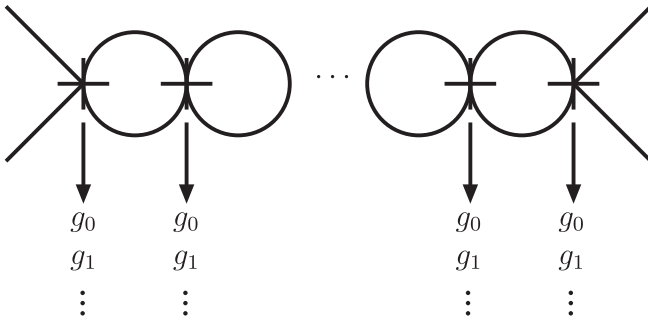

FIG. 5.   Insertions of counterterm Lagrangian vertices for the renormalization of the scattering amplitude.

$$\frac{s}{NF^2} \to \frac{s}{NF^2} G_0(s),$$

$$G_0(s) = \sum_{k=0}^{\infty} g_k \left(\frac{s}{F^2}\right)^k, \qquad (20)$$

with $g_0 = 1$, which gives, for the $T = 0$ amplitude,

$$A(s) = \frac{s}{NF^2} \frac{G_0(s)}{1 - \frac{sG_0(s)}{2F^2} J(s)}, \qquad (21)$$

or equivalently,

$$\frac{1}{A(s)} = \frac{NF^2}{s} \left[\frac{1}{G_0(s)} - \frac{sJ(s)}{2F^2} \right], \qquad (22)$$

written in a more suitable way to implement its renormalization, as we discuss below.

Now, we can renormalize the bare divergent (and scale-independent) LEC g_k correctly to absorb order by order the loop divergences coming from the $J(s)$ function. Thus, we denote $g_k^R(\mu)$ for $k \geq 1$ the renormalized (and scale-dependent) couplings that are renormalized in terms of the g_j with $j = 0, \ldots, k$ (see details in the Appendix). Equivalently, we define the renormalized function

$$\frac{1}{G_R(s;\mu)} = \frac{1}{G_0(s)} - \frac{s}{2F^2} J_\epsilon(\mu) \qquad (23)$$

which, when replaced in (22), gives rise to the renormalized amplitude:

$$A_R(s) = \frac{s}{NF^2} \frac{G_R(s;\mu)}{1 - \frac{sG_R(s;\mu)}{32\pi^2 F^2} \ln\left(\frac{\mu^2}{-s}\right)}, \qquad (24)$$

where the subscript R is merely added to emphasize that the amplitude is finite. Recall also that the renormalized amplitude is independent of the scale μ, as it was from the original expression (21), the scale dependence of $J_\epsilon(\mu)$ being canceled by that of the renormalized $g_k^R(\mu)$.

The function $G_R(s;\mu)$ can also be written as a formal series in powers of s by expanding both sides of Eq. (23) using (20), so that

$$G_R(s;\mu) = \sum_{k=0}^{\infty} g_k^R(\mu) \left(\frac{s}{F^2}\right)^k. \qquad (25)$$

Taking $g_0^R(\mu) = 1$ would give the order-by-order renormalization of the g_k, presented explicitly in the Appendix up to $\mathcal{O}(s^3)$ [specifically (A3) and (A4)].

At $T \neq 0$, on general grounds, we should be able to renormalize the amplitude with $T = 0$ counterterms [38,39]. However, we notice that the renormalization of the four-pion vertex in (20) and (23) is not enough to

renormalize the thermal amplitude in (10) (even though the divergent part of the J integral is the same as at $T = 0$) unless powers of $f(I_\beta)$ were attached to the counterterm Lagrangians, something that would violate the above-mentioned $T \neq 0$ renormalization principle. Actually, things become more complicated since the Feynman rules arising from terms like (19) are not as simple as the $T = 0$ ones, which, in particular, means that a given diagram mixes different s^k powers.

In the Appendix we present a detailed analysis of the renormalization scheme that has to be applied to the $T \neq 0$ case. The main conclusion is that the thermal amplitude can be rendered finite with a $T = 0$ renormalization where not only the four-point vertex (20) is involved, but also all $2k + 4$-pion vertices of the NLSM Lagrangian (1) for arbitrary integer k as follows:

$$\frac{s}{(NF^2)^{k+1}} \rightarrow \frac{s}{(NF^2)^{k+1}} G_0^{k+1}(s). \qquad (26)$$

The above renormalization, which can be understood either in terms of an addition of effective diagrams renormalizing the vertices or as a formal renormalization of the metric function at the Lagrangian level (see the Appendix), amounts to the redefinition of the effective thermal vertex in Fig. 3 as given in (A14) when the corresponding tadpole diagrams are summed up. In fact, one can also arrive at the same four-pion effective vertex renormalization in (A14) starting by redefining the thermal effective vertex with an unknown bare function of s and T that absorbs the divergent part of the J integral in the total amplitude. Thus, we finally have for the thermal amplitude

$$A(p; T) = \frac{sG_0(s)f[G_0(s)I_\beta]}{NF^2} \frac{1}{1 - \frac{sG_0(s)f[G_0(s)I_\beta]}{2F^2} J(p; T)}. \qquad (27)$$

After using exactly the same renormalization method given in (23), we obtain a finite renormalized thermal amplitude given by

$$A_R(p; T) = \frac{sG_R(s; \mu)f[G_R(s; \mu)I_\beta]}{NF^2}$$
$$\times \frac{1}{1 - \frac{sG_R(s; \mu)f[G_R(s; \mu)I_\beta]}{2F^2} J_{\text{fin}}(p; T; \mu)}, \qquad (28)$$

where J_{fin} is the finite part of the thermal J function, defined in (13).

Recall that our final finite thermal amplitude (28) is also independent of the μ scale, as in the $T = 0$ case, since the dependence in J_{fin} cancels out that of $G_R(s; \mu)$ encoded by the finite renormalization constants $g_i^R(\mu)$ through (25). We also point out that the renormalization scheme discussed here is the same as for $T = 0$ and is of course consistent

with the previous analysis of the scattering amplitude in the large-N NLSM in [33], but at $T = 0$ it is enough to consider the four-point vertex renormalization (20) because the $2k + 4$ vertices with $k \geq 1$ simply do not show up in the scattering amplitude at leading $1/N$ order.

The renormalized thermal amplitude (28) is one of our main results. As it happened in the $T = 0$ case [33,34], the infinite couplings g_i^R parametrize different choices of effective theories sharing basic properties such as renormalizability, the lowest order energy expansion (low-energy theorems) and unitarity (see Sec. IV). Indeed, at $T = 0$ one can, for instance, choose the g_i^R to recover the amplitude of the LSM with explicit exchange of a scalar particle. An alternative approach, which is the one we follow here, is to fix the scale and the renormalization conditions such that only a finite number of the g_i^R are nonzero. In its simplest version, we can choose $g_{k \geq 1}^R(\mu) = 0$. It is not difficult to see that this condition is compatible with the renormalization conditions of the G_R function, namely, (23), and its corresponding renormalization group evolution [33], and it leaves the thermal amplitude as dependent only on two free parameters, μ and F:

$$A_R(p; T) = \frac{sf[I_\beta]}{NF^2} \frac{1}{1 - \frac{sf[I_\beta]}{2F^2} J_{\text{fin}}(p; T; \mu)}. \qquad (29)$$

We show in Sec. IV A that it is possible with this approach to fit scattering data fairly well, considering that this is a chiral-limit approach (the finite pion mass case has been analyzed with the same method in [34]). That will be enough for our present purposes since our main goal is to show that with a $T = 0$ amplitude which complies with the above physical requirements, we can obtain a thermal behavior compatible with different theoretical and lattice expectations regarding chiral symmetry restoration, as we discuss in Sec. V.

It is also important to stress that following the guiding principle that the $T = 0$ renormalization should be enough to render a finite amplitude [proven perturbatively up to $\mathcal{O}(s^3)$ in the Appendix], the insertion of counterterms with bare renormalization constants g_i, the subsequent absorption of the divergent part of the loop integrals to define the g_i^R and taking $g_{k>1}^R(\mu) = 0$ would have been equivalent to take the thermal amplitude (10) with J replaced by J_{fin}. What we have derived here is an explicit construction of such a renormalization scheme.

To end this section and before proceeding with the analysis of partial waves and thermal poles, we provide a first result related to the pion decay constant at finite temperature. Taking the low-energy limit of the thermal amplitude from its general renormalized form (28) gives simply

$$A_R(p;T) = \frac{s}{NF^2}\frac{1}{1-\frac{I_\beta}{F^2}} + \mathcal{O}(s^2/F^4), \qquad (30)$$

which we can compare with the low-energy expression of the scattering amplitude given by Weinberg's theorem [17] to define a T-dependent pion decay constant, namely,

$$A_R(p;T) \equiv \frac{s}{F_\pi^2(T)} + \mathcal{O}(s^2/F^4),$$

so that

$$F_\pi^2(T) = NF^2\left(1 - \frac{T^2}{12F^2}\right) = F_\pi^2(0)\left[1 - \frac{T^2}{4F_\pi^2(0)}\right]$$
$$(N=3), \qquad (31)$$

where we have used that $F_\pi(0) = \sqrt{N}F$. The result (31) coincides with the known ChPT result to $\mathcal{O}(T^2)$ [19] and with the leading N contribution studied in [35], which are additional consistency checks of our present analysis. A more careful analysis of F_π beyond $\mathcal{O}(s)$ would require us to analyze the residue of the axial-axial correlator [10,35].

IV. PARTIAL WAVE ANALYSIS AND UNITARITY

A. Fitting the $I = J = 0$ phase shift at $T = 0$

As discussed above, we fix the undetermined constants in the scattering amplitude from experimental information. For that purpose and for the subsequent analysis of the $f_0(500)$ pole and chiral restoration, we consider partial waves with well-defined values of total isospin I and angular momentum J, which at $T = 0$ are defined in the c.m. frame $\vec{p} = \vec{0}$:

$$a_{IJ}(s) = \frac{1}{64\pi}\int_{-1}^{1} T_I(s,\cos\theta)P_J(\cos\theta)d(\cos\theta), \quad (32)$$

where P_J are Legendre polynomials, θ is the scattering angle and T_I is a particular combination involving $A(s,t,u)$ [defined in (4)] which gives the scattering amplitude at given isospin I, with $t(s,\cos\theta)$, $u(s,\cos\theta)$ in the c.m. frame. The large-N analysis is specially adequate for the $I = J = 0$ channel (see below), which on the other hand, is the one in which we are interested in this work. In that case, we have

$$T_{I=0}(s,\cos\theta) = NA_R(s) + A_R(t) + A_R(u)$$
$$= N[A_R(s) + \mathcal{O}(1/N)], \qquad (33)$$

with $A_R(s)$ given for $T = 0$ in (24) and where we have made use of the fact that $A(s,t,u)$ depends only on s to leading order in $1/N$; consistently, we only take the leading order for the partial wave combination (33) as well. The

final result is that the $I = J = 0$ partial wave is independent of N (to leading order). At $T = 0$ we then have

$$a_{00}(s) = \frac{s}{32\pi F^2}\frac{G_R(s;\mu)}{1 - \frac{sG_R(s;\mu)}{32\pi^2 F^2}\ln(\frac{\mu^2}{-s})}. \qquad (34)$$

Recall that within the large-N framework, the other possible isospin channels for pion scattering, namely, $I = 1$ and $I = 2$, are subdominant since they are proportional to $1/N$. This analysis is therefore particularly suited for a_{00} [34] which for the thermal case is the most relevant one regarding chiral symmetry restoration from the point of view of thermodynamic quantities such as the scalar susceptibility, as explained above.

As discussed in Sec. III, we work within the minimal approach for which $g_k^R(\mu) = 0$ for $k \geq 1$ so that we end up with the $T = 0$ partial wave in (34) with $G_R = 1$. Defining the phase shift as customary for elastic channels $a_{IJ} = |a_{IJ}|e^{i\delta_{IJ}}$, we can use this result to try to fit experimental phase shift data. There are several comments that are pertinent at this point: First, the choice of data sets is delicate because there have been several experiments over the years with results sometimes incompatible among them for this channel. In addition, we have to take into account that we are working in the chiral limit, so we expect our amplitude to more naturally describe data sufficiently away from threshold, i.e., typically for large $\sqrt{s}/(2m_\pi)$. On the other hand, there is also a natural upper limit of applicability for $\sqrt{s}$, namely, below the next resonance mass in this channel, which is the $f_0(980)$. For this, we would need to include the strange sector. Thus, we have chosen as data for the fit the sets given by [49] in the $\sqrt{s}$ range 450–800 MeV. In addition, we also consider the parametrization of the scattering amplitude described in [50] in the same energy region. That parametrization provides a precise description of $\pi\pi$ scattering from a combined analysis based on dispersion relations and provides an accurate prediction of the $f_0(500)$ and $f_0(980)$ pole parameters. We do not include in the fit the recent (and also more precise) data of the NA48 experiment [51] which are very low-energy data below $\sqrt{s} \sim 400$ MeV. Those low-energy data are very well described by the parametrization [50]. In the fit to the parametrization [50], we select points with a 5 MeV energy interval and take into account the small uncertainties given in that paper.

Another important point is that, in principle, the values obtained for F in our fits should not be far from the physical value of the pion decay constant $F_\pi = \sqrt{N}F$. In the chiral limit, $F_\pi \simeq 87$ MeV [18,52], so F would be around $F_\pi/\sqrt{3} \simeq 51$ MeV. However, once again, it is important to stress that we are forcing our chiral limit amplitude to fit data for massive pions, and it is then not surprising that we need a higher value for F since mass corrections increase
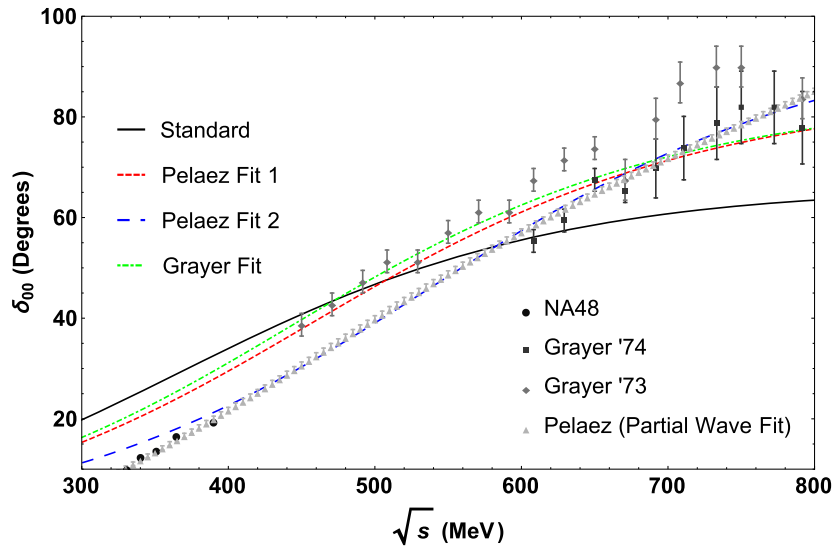
FIG. 6. The $I = J = 0$ channel phase shift for different fits, as explained in main text. The Peláez parametrization is given in [50], NA48 low-energy data in [51] and Grayer data in [49].

the F_π value; thus, we are encoding in F a great part of the uncertainty that we have in our chiral limit analysis.

In any case, it is not the purpose of this work to provide a very precise fit to experimental data, as in other unitarized or dispersive approaches [50,53] which can even be compared to lattice results by suitable mass extrapolations [54]. After all, this is just a two-parameter fit in the chiral limit. We just need some reasonable reference values for the parameters such that we dynamically generate a pole in the second Riemann sheet with consistent values for the pole position; thus, the thermal behavior corresponds to a physically realistic situation.

In Fig. 6 we show the $I = J = 0$ phase shift as a function of the c.m. energy obtained with our large-N amplitude with our best fits to Grayer data and to Peláez *et al.* parametrization. The corresponding fit parameters are given in Table I.

The behavior in this region is typically flat, compatible with having a wide resonance far from the real axis, in contrast with the $I = J = 1$ channel where the presence of the $\rho(770)$ narrow resonance is clearly evident for real s [53]. The fits are less sensitive to the value of μ, which is natural, taking into account that the dependence on that parameter is logarithmic. As commented above, the values for F are rather high, compared with the expected value, which is a consequence of dealing with the chiral limit. In the case of the fit to the points in [50], this effect is particularly notorious in the fit named "Peláez 2." However, we present the results of that fit anyway because of its

remarkably good accuracy to reproduce the parametrization [50], even in the very-low-energy region, where as commented, the approach was not meant to be applicable. In that sense, this fit better describes the scattering data for this channel, although the price to pay is an unnatural deviation in the pion decay constant. The chiral limit restriction, as well as other possible effects suppressed in the large-N limit, such as the t, u dependence of the amplitude, are encoded in that F value. Alternatively, in the fit named "Peláez 1," we fix the value $F = 65$ MeV such that we get a similar fit quality as the Grayer one, parametrized by R^2. Consequently, the values of μ obtained in those fits also remain close to each other. The uncertainties in F and μ given in Table I only include the error in the fit to the selected data and are therefore clearly underestimates, taking into account the additional sources of uncertainty mentioned above. In this context, it is also useful to compare with the values obtained in [34] for a fit including mass corrections, giving $F = 55.41$ MeV and $\mu = 775$ MeV. We denote the latter values as "standard values," whose corresponding curve with our chiral-limit amplitude is also depicted in Fig. 6. It is not surprising that this curve does not fit the data properly because the parameters are taken from the massive case fit. Finally, to check the robustness of our approach we have also tried to fit the same data sets by including one nonzero additional parameter g_1^R in G_R so that we now have a three-parameter fit. The result is that the best fit yields values for F and μ very close to those in Table I with g_1^R of the expected natural

TABLE I. Parameters for the Grayer and Peláez data fits and their respective coefficients of determination.

Parameters	Grayer	Peláez 1	Peláez 2
$F \pm \Delta F$ (MeV)	63.16 ± 1.62	65 (fixed)	75.98 ± 0.16
$\mu \pm \Delta\mu$ (MeV)	1523.35 ± 143.34	1607.89 ± 3.62	2763.51 ± 23.81
R^2	0.9958	0.9951	0.9999

order for the LEC [52] but compatible with zero. This is a consistency check of this approach, also reinforcing the idea commented in the Introduction that the $I = J = 0$ channel is less sensitive to the LEC than to the loop effects.

B. Unitarity at zero and finite temperature and the $f_0(500)$ pole

At $T = 0$ the unitarity condition for partial waves in elastic pion scattering reads $\mathrm{Im}\, a_{IJ}(s + i0^+) = \sigma(s, m_\pi)|a_{IJ}(s)|^2$ for $s \geq 4m_\pi^2$ (two-pion threshold), where σ is the two-pion phase space:

$$\sigma(s, m_\pi) = \sqrt{1 - \frac{4m_\pi^2}{s}}. \tag{35}$$

Equivalently, $T = 0$ unitarity reads $\mathrm{Im}[a_{IJ}^{-1}(s + i0^+)] = -\sigma(s, m_\pi)$. It is not difficult to see that the large-N a_{00} partial wave at $T = 0$ given in (34) satisfies this condition [recall that $G_R(s)$ is a real function] in the chiral limit:

$$\mathrm{Im}\left[\frac{1}{a_{00}(s + i0^+)}\right]$$
$$= -\frac{1}{\pi}\mathrm{Im}\left[\ln\left(\frac{\mu^2}{-s - i0^+}\right)\right] = -1 = -\sigma(s, 0) \quad \text{for } s \geq 0. \tag{36}$$

Exact unitarity is one of the prominent features of the large-N approach. Recall that in the standard ChPT series, unitarity holds only perturbatively order by order and demanding exact unitarity is what leads, for instance, to the IAM method.

What is even more interesting for our purposes is that there is a thermal unitarity relation which holds perturbatively in ChPT [22] and is given by $\mathrm{Im}\, a_{IJ}(s + i0^+; T) = \sigma_T(s, m_\pi)|a_{IJ}(s; T)|^2$ for $s \geq 4m_\pi^2$, where the partial waves at finite temperature are defined in the center-of-momentum frame $\vec{p} = \vec{0}$, i.e., the frame in which pions are at rest with the thermal bath, and where the thermal phase space σ_T is

$$\sigma_T(s, m_\pi) = \sigma(s, m_\pi)\left[1 + 2n_B\left(\frac{\sqrt{s}}{2}\right)\right]. \tag{37}$$

The Bose-Einstein correction in (37) can be interpreted as the difference of enhancement and absorption of scattering states in the thermal bath [22]. If this thermal perturbative relation is also imposed to hold for the full amplitude, one ends up with a unitarized thermal amplitude which gives rise to the T dependence of the $f_0(500)$ and $\rho(770)$ thermal poles [23,24,26].

An important result of the present work is that the thermal unitarity relation holds exactly for the large-N scattering amplitude, thus providing theoretical support to the previously mentioned works on this subject. This can be

readily checked from our previous results. From the definition of partial waves in (32) and (33), now with the thermal amplitude A_R in (28) at $\vec{p} = \vec{0}$, i.e., with J_{fin} given by (14) and (15), we have

$$a_{00}(s; T) = \frac{sG_R(s; \mu)f[G_R(s; \mu)I_\beta]}{32\pi F^2}$$
$$\times \frac{1}{1 - \frac{sG_R(s; \mu)f[G_R(s; \mu)I_\beta]}{32\pi^2 F^2}\left[\ln\left(\frac{\mu^2}{-s}\right) + 16\pi^2\delta J(s; T)\right]}. \tag{38}$$

Using (17), we now get

$$\mathrm{Im}\left[\frac{1}{a_{00}(s + i0^+; T)}\right] = -\frac{1}{\pi}[\pi + 16\pi^2\mathrm{Im}\delta J(s; T)]$$
$$= -\left[1 + 2n\left(\frac{\sqrt{s}}{2}\right)\right] = -\sigma_T(s, 0),$$

which is the thermal unitarity relation.

Unitarity allows us to define the Riemann second-sheet partial wave, both at $T = 0$ and at $T \neq 0$, when the amplitude is continued analytically to the s complex plane so that $\mathrm{Im}\, a^{II}(s - i0^+) = \mathrm{Im}\, a(s + i0^+)$ for $s > 4m_\pi^2$. This is achieved by $a^{II}(s; T) = a(s; T)/[1 - 2i\sigma_T a(s; T)]$. The second-sheet amplitude presents poles which correspond to the physical resonances, which in the case of pion scattering are the $f_0(500)$ ($I = J = 0$) and $\rho(770)$ ($I = J = 1$). The T-dependent poles can be extracted numerically by searching for zeros of $1/a^{II}(s; T)$ in the s complex plane. We denote the pole position as customary by $s_p(T) = [M_p(T) - i\Gamma_p(T)/2]^2$.

In the next section, we give the detailed results of the thermal pole evolution within our present large-N approach. Before that, in Table II we give the values of the $T = 0$ $f_0(500)$ pole, from the partial wave in (34), taking $G_R = 1$, with the different parameter sets of Table I, and in Fig. 7 we provide the surface-level plots for those poles. For comparison, we also present the results of the IAM in the chiral limit, using the same LEC as in previous works [26].

These values can be compared, for instance, with those obtained in the analysis [50] and given by $M_p = 457^{+14}_{-13}$ MeV, $\Gamma_p = 558^{+22}_{-14}$ MeV, compatible also with the PDG values $M_p \simeq 400\text{--}500\,\mathrm{MeV}$, $\Gamma_p = 400\text{--}700\,\mathrm{MeV}$ [11],

TABLE II. Values for masses and widths (in MeV) of the $f_0(500)$ pole at zero temperature.

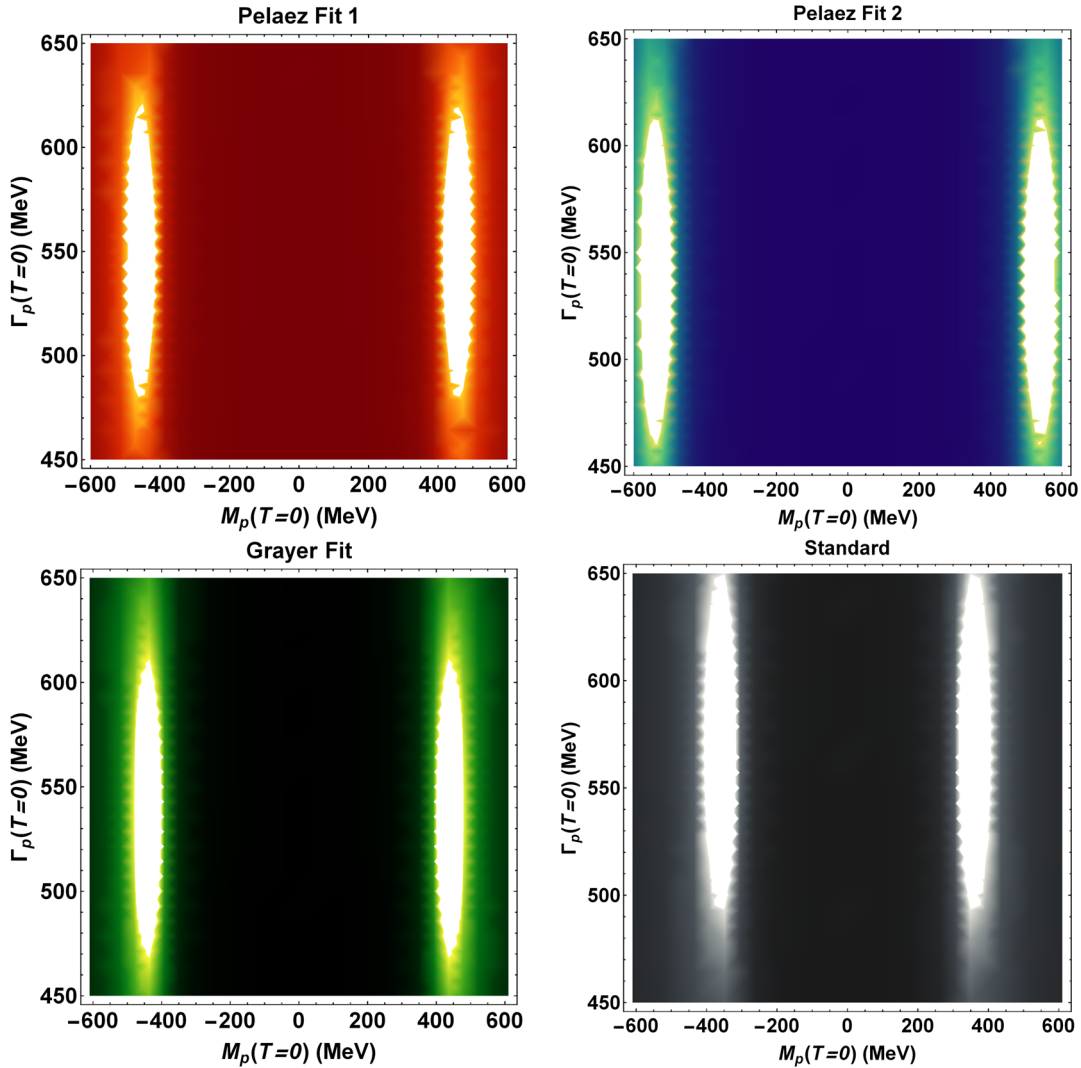| Fit	$M_P(T = 0)$	$\Gamma_P(T = 0)$
Grayer	438.81	536.47
Peláez 1	452.42	546.26
Peláez 2	535.53	534.59
IAM	406.20	522.70
Standard	356.97	566.05

FIG. 7.   Surface levels for $|a_{00}^{II}(s;T)|^2$ at $T = 0$ with Peláez 1,2, Grayer and standard fit parameters, respectively. The elliptic regions show the positions of the pole in the upper half of the second Riemann sheet.

with a large uncertainty and where the results of different analyses can be found. We refer also to the recent review [12] for updated results on the $f_0(500)$ pole parameters. The values we obtain here are compatible with those typically quoted in the literature, which is remarkable given that the uncertainties explained above related mostly to our chiral limit description. This is an important step in our analysis since we want our $T = 0$ values for the pole to be as close as possible to realistic values so that we can track its temperature evolution trustfully. In fact, we see that having already paid the price of somewhat increasing the value of F, the values for the mass and pole position are not far from those expected in the physical case. As a rule of thumb, we would expect that in the chiral limit, the pole mass would decrease (as it does for the quarklike component of this state) and the pole width would increase by a phase-space argument. That is the case, for instance, for the IAM pole, which in the massive case is at

$M_p = 441.47$ MeV, $\Gamma_p = 464.34$ MeV with the same LECs that give rise to the massless pole quoted in Table II. This is also the reason why the results in Table II for the "Standard" values, which correspond to a massive-pion fit, give in the chiral limit a smaller mass and higher width than the other large-N fits.

V. THERMAL EVOLUTION OF THE POLE AND CONNECTION WITH CHIRAL SYMMETRY RESTORATION

From our previous discussion, we can now follow the temperature evolution of the $f_0(500)$ pole and compare with previous analyses. In addition, following the proposal in [26], the thermal pole can be connected with chiral symmetry restoration (in the chiral limit) via the scalar susceptibility.

The results we obtain for the pole position parameters $M_p(T), \Gamma_p(T)$ in the second Riemann sheet at finite T from
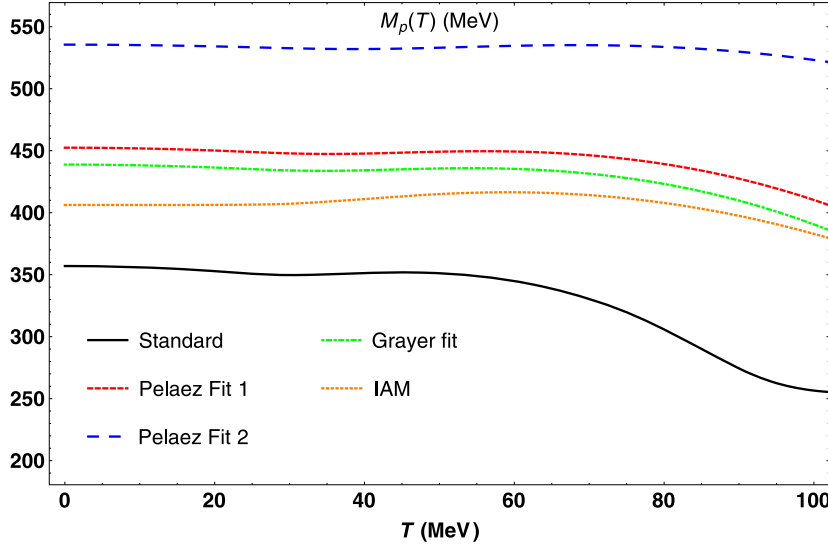
FIG. 8.   Mass of the $f_0(500)$ pole as functions of temperature when considering different fits in the large-N framework. We also compare with the IAM approach in the chiral limit.

the thermal partial wave in (38) (with $G_R = 1$) are given in Figs. 8 and 9. We also compare with the IAM approach in the chiral limit. A general tendency is observed regardless of the approach and the parameters, and it is that the pole mass decreases with T while the pole width increases. Thus, in the chiral limit at finite temperature, the $f_0(500)$ remains a wide resonance below the chiral transition. However, there are significant quantitative deviations when comparing different parameter sets, the results with the "Peláez 1" and "Grayer" fits and the IAM remaining reasonably close together.

What is more revealing is the behavior of $M_S^2 = M_p^2 - \Gamma_p^2/4$. This is nothing but the real part of the self-energy of the effective scalar state exchanged in pion scattering. On the other hand, the scalar susceptibility $\chi_S(T) = -\partial\langle \bar{q}q \rangle / \partial m_q$, with $\langle \bar{q}q \rangle$ the quark condensate and m_q the quark mass, is defined as the zero four-momentum scalar correlator and is saturated precisely by

M_S^2, assuming that the real part of the self-energy does not vary much in momentum from $p^2 = 0$ to $p^2 = s_p$ [26]. This is especially relevant close to the critical region where M_S^2 is expected to vanish, so

$$\frac{\chi_S(T)}{\chi_S(0)} = \frac{M_S^2(0)}{M_S^2(T)} = \frac{M_p^2(0) - \Gamma_p^2(0)/4}{M_p^2(T) - \Gamma_p^2(T)/4}. \tag{39}$$

Moreover, in [26] it has been shown that using the IAM scalar $f_0(500)$ thermal pole to saturate the scalar susceptibility through (39) precisely generates a unitarized version of χ_S which develops a maximum very close to the critical point predicted by lattice analysis, i.e., $T_c \sim 155$ MeV, in the physical massive case where the transition is believed to be a crossover. In that case, the maximum comes from a combination of the dropping $M_p(T)$ behavior and the $\Gamma_p(T)$ behavior, which grows at low and moderate temperatures due to the phase space increasing, but it drops near
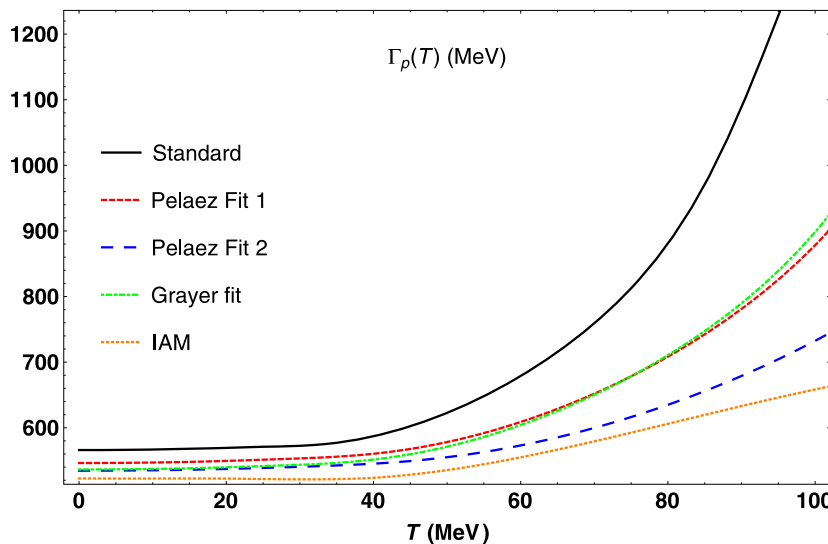

FIG. 9.   Width of the $f_0(500)$ pole as functions of temperature when considering different fits and the IAM in the chiral limit.
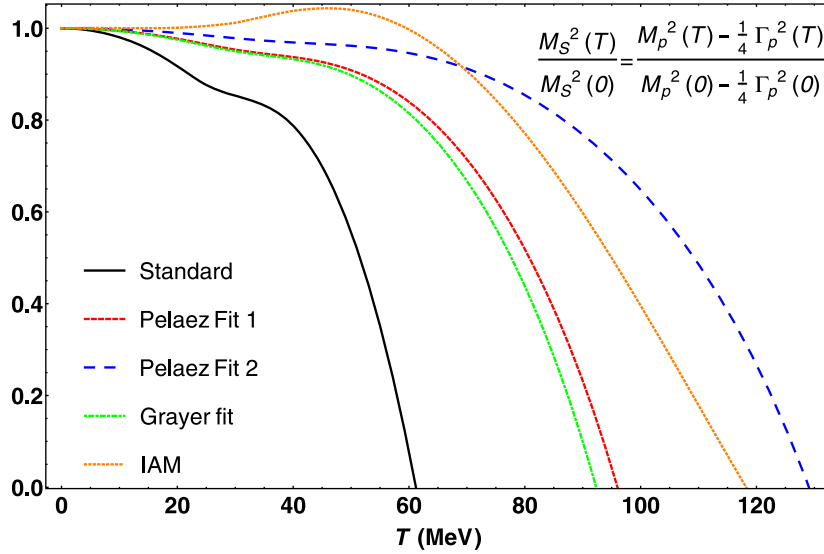
FIG. 10. Normalized scalar mass squared (inverse scalar susceptibility) as a function of the temperature for different parameter sets and the IAM.

$$\frac{M_S^2(T)}{M_S^2(0)} = \frac{M_p^2(T) - \frac{1}{4}\Gamma_p^2(T)}{M_p^2(0) - \frac{1}{4}\Gamma_p^2(0)}$$

the transition where mass reduction is dominant. In our present approach in the chiral limit, $\Gamma_p(T)$ grows monotonically, so the thermal phase space dominates over mass reduction in the temperature range of interest.

In the chiral limit the transition should be a second-order one, so such a maximum should become a pole, accompanied by a significant reduction in T_c. We show our results for $M_S^2(T)/M_S^2(0)$ in Fig. 10. A clear dropping behavior vanishing at T_c is observed, corresponding to a chiral restoration second-order continuous phase transition, according to our previous discussion. The values of T_c obtained for different parameters are given in Table III. We also compare with the IAM in the chiral limit, which shows a similar dropping behavior, although qualitatively different in the intermediate temperature region.

Let us now comment on these results. A first interesting consistency check, from the formal point of view, is that the result for T_c we obtain here is independent of N for large N since it is extracted from an N-independent quantity, namely, the partial wave (38). This is consistent with the T_c extracted from the partition function, which to leading order in $1/N$ is also N independent and is given by $T_c^2 = 12F^2$ in the chiral limit [10,36]. That also happens in other approaches such as ChPT, where the thermal loop corrections to the quark condensate increase proportionally to N

but are divided by $F_\pi^2 \sim NF^2$ [19,20]. However, our numerical values for T_c extracted in the way we have just discussed are remarkably closer to the range expected from lattice simulations than the large-N value just mentioned. As commented in the Introduction, phenomenologically we expect a T_c value of about 80% of the massive case, namely, around 120 MeV. In addition, the predictions from our large-N approach are very close to the IAM one, which is formulated for $N = 3$. Thus, with our approach we obtain results closer to the real $N = 3$ world, even though they come from the leading order in $1/N$. Generically speaking, we would expect up to 30% uncertainties for $N = 3$, coming from the neglected $1/N$ corrections, but we see that our results are even better than this. The key point is that, apart from the large-N resummation, which incorporates important formal properties such as thermal unitarity, we have chosen our parameters to obtain reliable values for the phase shifts and pole at $T = 0$, i.e., close to the physical case. In this sense, it is important to remark that getting $T = 0$ pole values quite close to the physical (massive) ones, by increasing the F value, does not imply that the T evolution of the pole towards chiral restoration should be like the massive case, e.g., for T_c, since there are genuine massive thermal effects that we are neglecting when taking the chiral limit, like the combined dependence of thermal distribution functions on mass and temperature [20]. For that reason, we get T_c values closer to the expected chiral limit ones. We also mention at this point that studies of the chiral phase transition based on the renormalization group yield $T_c \simeq 100.7$ MeV in the chiral limit [7], also very close to our present analysis.

Another chiral-restoration property we can examine is the scaling law for the scalar susceptibility defined through (39), i.e., calculating the critical exponent γ determined as $\chi_S(T)/\chi_S(0) \sim (T_c - T)^{-\gamma_\chi}$ for $T \to T_c^-$. The results for the best fits are shown in Table IV. We can compare

TABLE III. Values for the chiral critical temperature obtained for different parameter sets and the IAM.

Parameter set	T_c (MeV)
Grayer	92.33
Peláez 1	96.00
Peláez 2	129.07
IAM	118.23
Standard	61.20

TABLE IV. Critical exponents for χ_S extracted from our results in Fig. 10.

Fit	γ_χ	R^2
Grayer	0.875	0.99987
Peláez 1	0.938	0.99997
Peláez 2	0.919	0.99995
IAM	1.012	1
Standard	0.842	0.99728

this analysis, on the one hand, with the exact result for the nonlinear $O(N)$ model for $N \to \infty$ in four dimensions, $\gamma_\chi^{O(\infty)4D} = 1 + \mathcal{O}(1/N^2)$ [47]. On the other hand, the critical exponent of the $O(4)$ three-dimensional Heisenberg model, which lattice QCD results resemble within uncertainties [8], is $\gamma_\chi^{O(4)3D} \simeq 0.54$ for $T < T_c$ in the chiral limit [8,55]. Our results and the IAM one lie close to those values, then providing a consistency check of our approach to define the scalar susceptibility from the $f_0(500)$ pole.

VI. CONCLUSIONS

We have studied pion scattering in the large-N $O(N + 1)/O(N)$ model at finite temperature in the chiral limit and its consequences regarding the $f_0(500)$ pole and chiral symmetry restoration. Our analysis gives rise to interesting theoretical and phenomenological results, consistent with previous analysis and lattice data.

After calculating the relevant Feynman diagrams, which include an effective thermal vertex from tadpole resummation, an important part of our work has been devoted to show that it is possible to find a renormalization scheme rendering the thermal amplitude finite with a $T = 0$ renormalization of the corresponding vertices. This is a nontrivial extension of the $T = 0$ renormalization of the scattering amplitude since the breaking of Lorentz covariance in the thermal bath induces crossed terms between tadpolelike and J_T loop functions. In the low-energy expansion of the model, up to $\mathcal{O}(s^3)$, we have checked explicitly this renormalization scheme, providing a diagrammatic and Lagrangian interpretation.

Another relevant result is that the large-N thermal amplitude exactly satisfies the thermal unitarity relation, imposed in previous works as a physical condition for the exact amplitude. Its low-energy properties are also preserved, being consistent, for instance, with the thermal dependence of the pion decay constant.

By a suitable choice of the low-energy constants, similarly to the $T = 0$ case, compatible with the scale evolution of the renormalized couplings, we end up with a phenomenological unitary amplitude depending only on two parameters, F and μ. By fitting those parameters to experimental data in the $I = J = 0$ channel, which is more reliable for data not very close to threshold in the elastic region, we reproduce the pole position of the $f_0(500)$ in the second Riemann sheet fairly consistently with PDG values and recent determinations. The chiral limit character of our approach implies a larger value for F than phenomenologically expected, but it allows us to obtain pole position parameters M_p, Γ_p closer to the physical case. The fits to data are actually very good in the chosen region, precisely the most relevant energy range concerning this resonant state.

Once the $T = 0$ pole was fixed to physical values, we studied its evolution with temperature. The $f_0(500)$ pole remains a wide state for all the temperature range of interest, the real and imaginary parts $M_p(T)$ and $\Gamma_p(T)$ behaving similarly to the IAM analysis, showing the signature of chiral restoration. In order to explore this further, we define a scalar susceptibility $\chi_S(T)$ saturated by the inverse of $M_S^2(T) = M_p^2(T) - \Gamma_p^2(T)/4$, corresponding to the real part of the scalar state self-energy at zero four-momentum, which diverges at a given T_c with a power law, as it corresponds to a continuous second-order phase transition in the chiral limit. The values obtained for T_c, as well as the critical exponent of χ_S, are consistent with those obtained with other analytical approaches, such as the IAM, and with lattice analysis, being compatible with an $O(4)$ scaling. The combination of the large-N framework with the phenomenological features of the $f_0(500)$ pole allows us to improve the predictions of previous approaches based on the partition function. Thus, we obtain a very reasonable description of the chiral restoration transition within this approach, given the different uncertainties involved, such as possible $1/N$ corrections near the physical $N = 3$ case or the absence of heavier degrees of freedom, which should play an important role near the transition and improve our simple pion gas scenario.

APPENDIX: DETAILS OF THE RENORMALIZATION PROCEDURE

A Lagrangian of the form (19) gives rise to the Feynman rule $2^k[(p_A \cdot p_B)^k(p_C \cdot p_D) + (p_A \cdot p_B)(p_C \cdot p_D)^k]\delta_{AB}\delta_{CD}$ where $p_{A,B,C,D}$ are the four-momenta of the four legs and A, B, C, D their isospin indices. We consider insertions of these counterterms in diagrams of the form depicted in Fig. 5, which will be the dominant ones in $1/N$. For those insertions, we then have to deal with integrals of the type

$$
\begin{aligned}
J_n(p, T) &= \int_T d^D q \frac{[q \cdot (p-q)]^n}{q^2(p-q)^2} \\
&= \frac{1}{2^n} \int_T d^D q \frac{[s - q^2 - (p-q)^2]^n}{q^2(p-q)^2} \\
&\qquad (n = 0, 1, 2...),
\end{aligned} \tag{A1}
$$

where $\int_T d^D q$ is short for $T\sum_n \int \frac{d^{D-1}\vec{q}}{(2\pi)^{D-1}}$, $q_0 = i\omega_n$, $p_0 = i\omega_m$ and $s = p^2$ (after analytic continuation). The case $n = 0$ corresponds to $J_0 = J(i\omega_m, |\vec{p}|; T)$ in (12).

First, consider the $T = 0$ case. Since $\int dq q^\alpha = 0$ in DR [48], the only remaining terms after expanding the numerator in (A1) are the s^n one and the contributions $\int \frac{q^{2j}}{(p-q)^2} = \int \frac{(p+q)^{2j}}{q^2}$ and $\int \frac{(p-q)^{2j}}{q^2}$. The latter vanish also in DR since $\int dq \frac{q_1^{N_1} \cdots q_D^{N_D}}{q^2}$ (N_i even) is formally proportional to $\int dq \frac{q^N}{q^2} = 0$, with $N = \sum_i N_i$ [using the standard parametrization for $1/q^2 = \int_0^\infty d\lambda \exp(-\lambda q^2)$]. Therefore, in that case we simply have

$$
J_n(s; T = 0) = \left(\frac{s}{2}\right)^n J(s), \tag{A2}
$$

with $J(s)$ given in (6).

Thus, at $T = 0$, any g_k insertion is proportional to s^{k+1}, regardless of the vertex being internal of external. As stated in the main text, this allows us to renormalize the amplitude at every order. As an example, let us show here the diagrams contributing up to $\mathcal{O}(s^3)$ at $T = 0$, which are those shown in Fig. 11 and where we have indicated the order of every diagram. Summing up these contributions, the amplitude is finite with the following renormalization of g_1, g_2:

$$
g_1^R(\mu) = g_1 + \frac{1}{2}J_\epsilon(\mu), \tag{A3}
$$

$$
\begin{aligned}
g_2^R(\mu) &= g_2 - \frac{1}{4}[J_\epsilon(\mu)]^2 + g_1^R(\mu)J_\epsilon(\mu) \\
&= g_2 + \frac{1}{4}[J_\epsilon(\mu)]^2 + g_1 J_\epsilon(\mu).
\end{aligned} \tag{A4}
$$

When the $T = 0$ amplitude is written in terms of the renormalized constants, it adopts the form (24), where to this order $G_R(s; \mu) = 1 + g_1^R(\mu)\frac{s}{F^2} + g_2^R(\mu)\frac{s^2}{F^4} + \mathcal{O}(s^3)$. As it was assured above, this is equivalent to renormalizing the amplitude by the functional renormalization of the four-pion vertex given in Eqs. (20) and (23).

At $T \neq 0$, there are additional complications that need to be analyzed in detail. First of all, the simple relation (A2) for the integrals J_n in (A1) no longer holds. Namely, for $n = 1$ we get directly from (A1)

(a) $\mathcal{O}(s)$ (b) $\mathcal{O}(s^2)$ (c) $\mathcal{O}(s^2)$

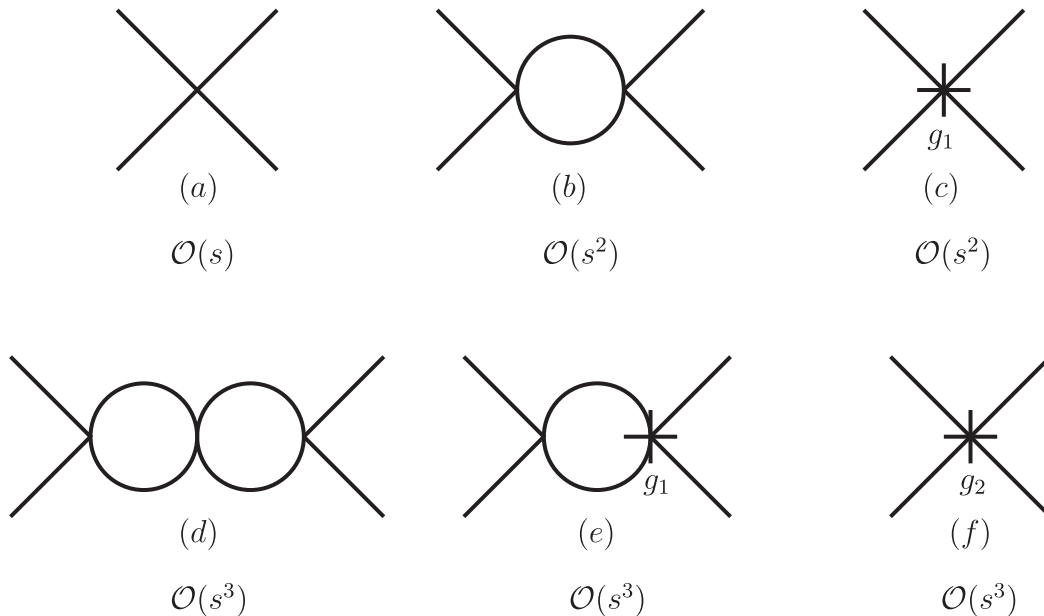(d) $\mathcal{O}(s^3)$ (e) $\mathcal{O}(s^3)$ (f) $\mathcal{O}(s^3)$

FIG. 11. Diagrams up to $\mathcal{O}(s^3)$ for the renormalized amplitude at $T = 0$. We plot the different topological configurations contributing, so that diagram (e) is multiplied by two, corresponding to the possible vertex insertions of g_1.

$$J_1(p;T) = \frac{1}{2}[sJ_0 + 2I_\beta], \qquad \text{(A5)}$$

with I_β the tadpole integral in (9), while for $n = 2$,

$$J_2(p,T) = \frac{1}{4}\left[s^2 J_0 + 4sI_\beta + \int_T d^D q \frac{(p+q)^2}{q^2} \right.$$
$$\left. + \int_T d^D q \frac{(p-q)^2}{q^2}\right] = \frac{s}{4}[sJ_0 + 2I_\beta], \qquad \text{(A6)}$$

where we have used that in DR $\int_T d^D q \, q^{2n} = \int_T d^D q (p - q)^{2n} = 0$ for $n = 0, 1, 2, \dots$ (although not for any real n as in the $T = 0$ case) since $\int d^{D-1}\vec{q}|\vec{q}|^{2k} = 0$ for $k = 0, 1, 2, \dots$. Note also that in (A6), the two contributions $\int_T d^D q \frac{p \cdot q}{q^2}$ cancel among them, and also independently by parity. However, this does not happen for $n \geq 3$, meaning that the J_n's are not simply linear combinations of J_0 and I_β as in the previous cases. For instance, for $n \geq 3$ the following integral contributes:

$$\int_T d^D q \frac{(p \cdot q)^2}{q^2} = p_\mu p_\nu I^{\mu\nu}(T) = -\omega_m^2 I^{00}(T) - |\vec{p}|^2 I_s(T),$$
$$\qquad \text{(A7)}$$

with $I^{\mu\nu} = \int_T d^D q \frac{q^\mu q^\nu}{q^2}$ and $I_s = \frac{1}{D-1} I_j^j$. At $T = 0$, one has $I^{\mu\nu} = g^{\mu\nu} \frac{1}{D} \int d^D q = 0$ in DR, but at $T \neq 0$ the timelike and spacelike contributions decouple, from the loss of Lorentz covariance in the thermal bath, and they are, in general, nonzero. Besides,

$$I_s(T) = \frac{1}{D-1} \int_T d^D q |\vec{q}|^2 \int_0^\infty d\lambda e^{-\lambda(\omega_n^2 + |\vec{q}|^2)}$$
$$= \frac{1}{(4\pi)^{\frac{D-1}{2}}} \frac{T}{2} \sum_{n=-\infty}^\infty \int_0^\infty d\lambda e^{-\lambda \omega_n^2} \lambda^{-1-\frac{D-1}{2}}$$
$$= I_s(0) + \frac{1}{(4\pi)^{\frac{D}{2}}} \sum_{k=1}^\infty \int_0^\infty d\lambda \lambda^{-1-\frac{D}{2}} e^{-\frac{k^2}{4T^2\lambda}}$$
$$= \frac{1}{2} g_0(0,T) = \frac{\pi^2}{90} T^4, \qquad \text{(A8)}$$

where we have made use of the standard Feynman parametrization as well as Poisson's summation formula $\sum_n F(n) = \sum_k \int_{-\infty}^\infty dx F(x) \exp(2\pi i k x)$. The function $g_0(M,T)$ is defined in [20]. On the other hand, using again the DR properties, $I^{00}(T) = -(D-1)I_s(T)$. Note that $I_s(0) = 0$, so these pure thermal contributions would not give rise to new types of divergences, i.e., different from those coming from the standard loop integral in (13).

Therefore, the Feynman rules at $T \neq 0$ for g_k insertions change with respect to the $T = 0$ ones. Namely, a g_k insertion in the generic diagram of Fig. 5 produces an integral of the type (A1) for the internal loop momenta q and then is not equivalent to a simple s^k power as for $T = 0$.

One of the consequences of the above results is that when considering all the diagrams contributing to a given s^k order, the s and T^2 powers mix, so a larger number of diagrams has to be considered. In Fig. 12 we have displayed all the diagrams that would give $\mathcal{O}(s^3)$ contributions, all of them including g_1 and g_2 insertions according to the results (A5) and (A6). The vertex with no $g_{1,2}$ insertions is the effective thermal vertex in Fig. 3. Attached to each diagram, we have indicated the different powers of $s^n I_\beta^m$ that it gives rise to.

We have calculated all diagrams in Fig. 12 with the Feynman rules discussed above. The result is that the amplitude to that order remains finite with the same $T = 0$ renormalizations of g_1 and g_2 given in (A3) and (A4), which is a nontrivial consistency check. Furthermore, the analysis of the result reveals some interesting features that will shed light on the renormalization scheme to be followed in the general case.

First of all, we show the $\mathcal{O}(s^2)$ calculation. In addition to diagrams (a), (b), (c) of Fig. 12, which are the counterparts of (a), (b), (c) in Fig. 11 with the thermal vertex, we also have to consider diagram (e) in Fig. 12 since it includes a $I_\beta s^2$ contribution, as well as diagram (g), whose $I_\beta^2 s^2$ part has to be taken into account. Altogether, we obtain for the amplitude at that order

$$A(p;T) = \frac{s}{NF^2} f(I_\beta)\left\{1 + \frac{s}{2F^2} f(I_\beta)[2g_1 + J(p;T)]\right\} + \mathcal{O}(s^3)$$
$$= \frac{s}{NF^2} f(I_\beta)\left\{1 + \frac{s}{2F^2} f(I_\beta)[2g_1^R(\mu) + J_{fin}(p;T;\mu)]\right\} + \mathcal{O}(s^3), \qquad \text{(A9)}$$

where we have separated the loop integral into its divergent and finite parts according to (13) and (7) and we have used exactly the same renormalization of the g_1 constant as for $T = 0$, namely, (A3). The thermal amplitude in (A9) is

explicitly finite and scale independent to this order. Moreover, note that we can write the thermal amplitude to that order in a form similar to the renormalized $T = 0$ case in (21) as follows:
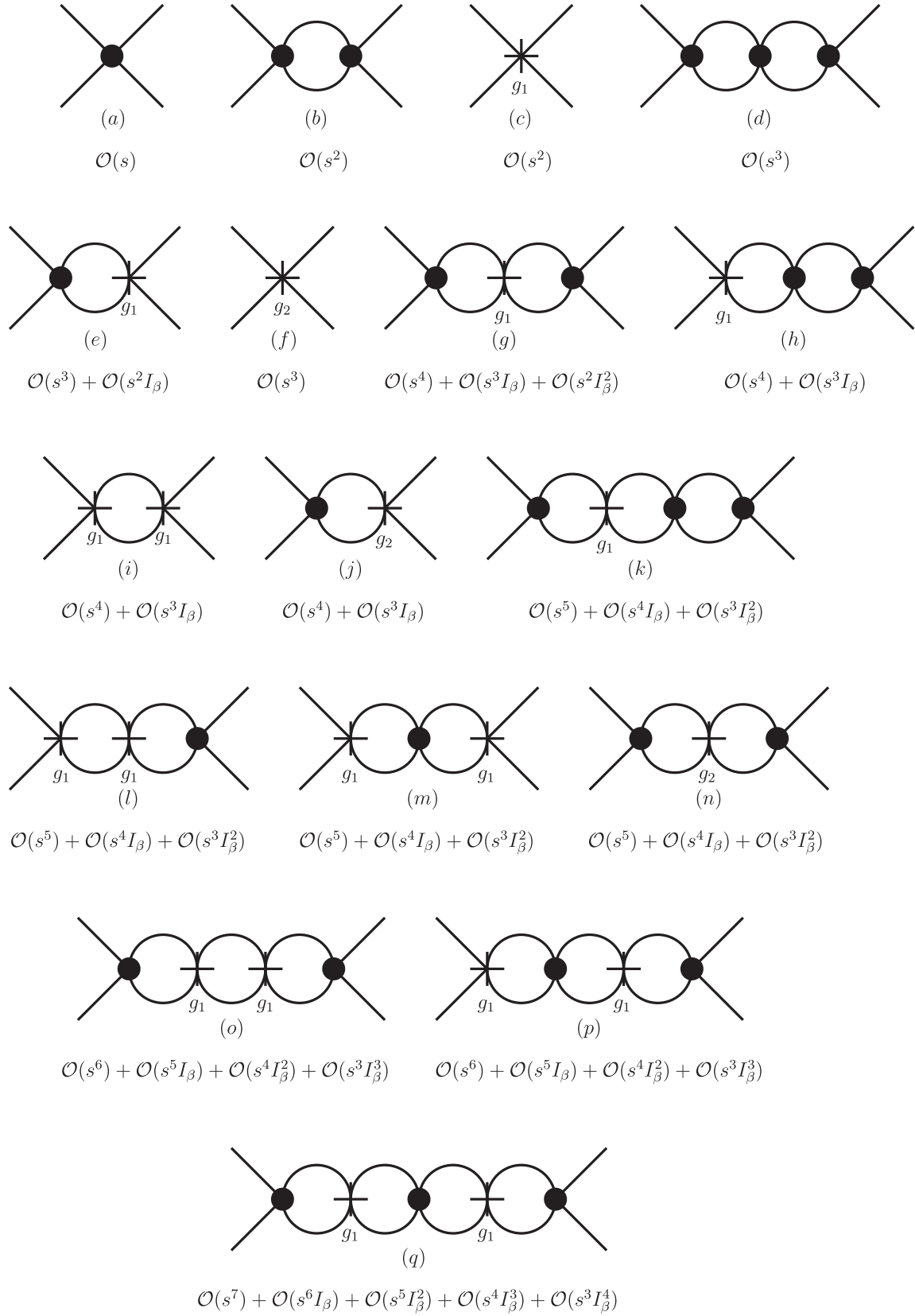
FIG. 12.   Diagrams up to $\mathcal{O}(s^3)$ for the renormalized amplitude at $T \neq 0$. We plot the different topological configurations contributing, so diagrams (e), (h), (j), (k), (l), (p) are multiplied by two, corresponding to the possible vertex insertions.

$$A(p;T) = \frac{sG_0(s)}{NF^2}\frac{1}{1-G_0(s)I_\beta/F^2}\frac{1}{1-\frac{sG_0(s)}{2F^2}\frac{1}{1-G_0(s)I_\beta/F^2}J(p;T)} + \mathcal{O}(s^3)$$

$$= \frac{sG_0(s)f[G_0(s)I_\beta]}{NF^2}\frac{1}{1-\frac{sG_0(s)f[G_0(s)I_\beta]}{2F^2}J(p;T)} + \mathcal{O}(s^3), \tag{A10}$$

with $G_0(s)$ given by the same expression as in the $T=0$ analysis (20) to this order, i.e., $G_0(s) = 1 + g_1(s/F^2) + \mathcal{O}(s^2)$. Thus,

$$\frac{1}{A(p;T)} = \frac{NF^2}{s}\left[\frac{1}{G_0(s)f[G_0(s)I_\beta]} - \frac{sJ(p;T)}{2F^2}\right] = \frac{NF^2}{s}\left[\frac{1}{G_0(s)} - \frac{I_\beta}{F^2} - \frac{sJ(p;T)}{2F^2}\right]$$

$$= \frac{NF^2}{s}\left[\frac{1}{G_R(s;\mu)} - \frac{I_\beta}{F^2} - \frac{sJ_{\text{fin}}(p;T;\mu)}{2F^2}\right]$$

$$\Rightarrow A_R(p;T) = \frac{sG_R(s;\mu)f[G_R(s;\mu)I_\beta]}{NF^2}\frac{1}{1-\frac{sG_R(s;\mu)f[G_R(s;\mu)I_\beta]}{2F^2}J_{\text{fin}}(p;T;\mu)} + \mathcal{O}(s^3). \tag{A11}$$

Here G_R is written in terms of G_0 as in (23), so that $G_R(s) = 1 + g_1^R(\mu)(s/F^2) + \mathcal{O}(s^2)$, which renders the amplitude finite.

The same structure is obtained when we calculate up to $\mathcal{O}(s^3)$ and then take into account the corresponding contributions from the diagrams in Fig. 12. Now we obtain

$$A(p;T) = \frac{s}{NF^2}f(I_\beta)\left\{1 + \frac{s}{2F^2}f(I_\beta)[2g_1 + J(p;T)] + \frac{s^2}{F^4}f^2(I_\beta)\left[g_1J(p;T) + \frac{1}{4}J^2(p;T) + g_2\left(1 - \frac{I_\beta}{F^2}\right) + g_1^2\frac{I_\beta}{F^2}\right]\right\} + \mathcal{O}(s^4)$$

$$= \frac{s}{NF^2}f(I_\beta)\left\{1 + \frac{s}{2F^2}f(I_\beta)[2g_1^R(\mu) + J_{\text{fin}}(p;T;\mu)] + \frac{s^2}{F^4}f^2(I_\beta)[g_1^R(\mu)J_{\text{fin}}(p;T;\mu) + \frac{1}{4}J_{\text{fin}}^2(p;T;\mu)\right.$$

$$\left. + g_2^R(\mu)\left(1 - \frac{I_\beta}{F^2}\right) + [g_1^R(\mu)]^2\frac{I_\beta}{F^2}\right]\right\} + \mathcal{O}(s^4), \tag{A12}$$

which is again finite with the renormalizations (A3) and (A4) and can also be written as

$$A(p;T) = \frac{sG_0(s)f[G_0(s)I_\beta]}{NF^2}\frac{1}{1-\frac{sG_0(s)f[G_0(s)I_\beta]}{2F^2}J(p;T)} + \mathcal{O}(s^4)$$

$$\Rightarrow A_R(p;T) = \frac{sG_R(s;\mu)f[G_R(s;\mu)I_\beta]}{NF^2}\frac{1}{1-\frac{sG_R(s;\mu)f[G_R(s;\mu)I_\beta]}{2F^2}J_{\text{fin}}(p;T;\mu)} + \mathcal{O}(s^4), \tag{A13}$$

with $G_0(s) = 1 + g_1(s/F^2) + g_2(s/F^2)^2 + \mathcal{O}(s^3)$ and $G_R(s;\mu) = 1 + g_1^R(\mu)(s/F^2) + g_2^R(\mu)(s/F^2)^2 + \mathcal{O}(s^3)$.

Therefore, from the previous expressions we observe that the $T \neq 0$ renormalization is equivalent to the following renormalization of the four-pion thermal effective vertex:

$$\frac{s}{NF^2}f(I_\beta) \rightarrow \frac{s}{NF^2}G_0(s)f[G_0(s)I_\beta]. \tag{A14}$$

What is interesting for our purposes is that the renormalization given in (A14) can actually be achieved by a $T=0$ renormalization of each of the $2n$-pion vertices in the original Lagrangian by assigning them a $G_0^{n-1}(s)$ factor in momentum space, as displayed in Table V, thus generalizing the 4π vertex renormalization in (20).

It is actually possible to trace the origin of this renormalization scheme in terms of the contributing diagrams. Consider, for instance, diagrams with just one g_1 insertion. At $\mathcal{O}(s^2)$, one has to sum the contributions to the amplitude from diagrams (c), (e) and (g) in Fig. 12, namely,

$$\frac{g_1 s^2}{NF^4}\left[1 + \frac{2x}{1-x} + \frac{x^2}{(1-x)^2}\right] = \frac{g_1 s^2}{NF^4}\sum_{k=1}^{\infty} kx^{k-1}, \tag{A15}$$

TABLE V. Feynman rule renormalization for the interaction vertices of the Lagrangian (1) for $\pi\pi$ scattering at large N.

Vertex	Lagrangian	Bare rule	Renormalized rule
4 pions	$-\frac{\pi^2\Box\pi^2}{8NF^2}$	$\frac{s}{NF^2}$	$\frac{sG_0(s)}{NF^2}$
6 pions	$-\frac{(\pi^2)^2\Box\pi^2}{16(NF^2)^2}$	$\frac{s}{(NF^2)^2}I_\beta$	$\frac{sG_0^2(s)}{(NF^2)^2}I_\beta$
$2k+4$ pions	$-\frac{(\pi^2)^{k+1}\Box\pi^2}{8(k+1)(NF^2)^{k+1}}$	$\frac{s}{(NF^2)^{k+1}}I_\beta^k$	$\frac{sG_0^{k+1}(s)}{(NF^2)^{k+1}}I_\beta^k$

with $x = I_\beta/F^2$. Now, the infinite contributions in the sum in (A15) amount to four-point diagrams with $k-1$ tadpole contractions ($k = 1, 2, \ldots$), i.e., like the diagrams in Fig. 3 with a $kg_1\frac{s^2}{NF^4}$ vertex. But we can interpret each of those diagrams as the contribution to the scattering amplitude of a multiplicative renormalization of the $(2 + 2k)$-pion vertex of the Lagrangian (1) given by $\frac{s}{(NF^2)^k} \rightarrow \frac{s}{(NF^2)^k}[1 + kg_1\frac{s}{F^2}] + \mathcal{O}(s^3) = \frac{s}{(NF^2)^k}G_0^k(s) + \mathcal{O}(s^3)$, for which closing $2(k-1)$ lines gives $(NI_\beta)^{k-1}$ to leading order in N. This is precisely the rule given in Table V.

We have checked that we find the same rule by analyzing the remaining g_i insertions in the graphs in Fig. 12.

Specifically, the $\mathcal{O}(s^3)$ contribution with one g_1 insertion [diagrams (e), (g), (h) and (k)] gives the renormalization rule in Table V for diagrams with the one-loop J function, the $\mathcal{O}(s^3)$ with one g_2 insertion [diagrams (j) and (n)] give the linear part in g_2 of the $G_0^k(s)$ contribution which we have just analyzed above to $\mathcal{O}(s^2)$, while the $\mathcal{O}(s^3)$ with two g_1 insertions [diagrams (i), (l), (m), (o), (p), (q)] reproduce precisely the g_1^2 part of those $G_0^k(s)$ terms. Therefore, in this way we are able to reinterpret all g_i insertions in Fig. 12 giving $s^n I_\beta^m$ mixed powers with $n = 2$, 3 and $m = 1, 2, 3, 4$, in terms of the T-independent renormalization scheme in Table V and (A14), from the contributing diagrams without mixed terms. For higher insertions, we would need higher order diagrams with respect to those of Fig. 12, i.e., up to $\mathcal{O}(s^4)$.

The crucial conclusion is that, following the above renormalization scheme also in the general nonperturbative case, namely, starting from the full amplitude (10), yields a finite scattering amplitude with a $T = 0$ renormalization, as discussed in the main text.

Finally, let us comment about this renormalization scheme from the point of view of the effective Lagrangian. For that purpose, let us write down the expansion of the NLSM Lagrangian (1) as

$$
\begin{aligned}
\mathcal{L} &= \frac{1}{2}g_{ab}(\boldsymbol{\pi})\partial_\mu\boldsymbol{\pi}^a\partial^\mu\boldsymbol{\pi}^b = \frac{1}{2}\left(\delta_{ab} + \frac{1}{NF^2}\frac{\boldsymbol{\pi}_a\boldsymbol{\pi}_b}{1-\boldsymbol{\pi}^2/NF^2}\right)\partial_\mu\boldsymbol{\pi}^a\partial^\mu\boldsymbol{\pi}^b \\
&= \frac{1}{2}\left[\partial_\mu\boldsymbol{\pi}_a\partial^\mu\boldsymbol{\pi}^a + \frac{1}{4}\sum_{k=0}^{\infty}\frac{(\boldsymbol{\pi}^2)^k(\partial_\mu\boldsymbol{\pi}^2)(\partial^\mu\boldsymbol{\pi}^2)}{(NF^2)^{k+1}}\right] \\
&= -\frac{1}{4}\left[1 + \frac{1}{2}\sum_{k=0}^{\infty}\frac{1}{k+1}\left(\frac{\boldsymbol{\pi}^2}{NF^2}\right)^{k+1}\right]\Box\boldsymbol{\pi}^2 = -\frac{1}{4}\left[1 - \frac{1}{2}\ln\left(1 - \frac{\boldsymbol{\pi}^2}{NF^2}\right)\right]\Box\boldsymbol{\pi}^2,
\end{aligned}
\tag{A16}
$$

where we have used

$$
(\boldsymbol{\pi}^2)^j(\partial_\mu\boldsymbol{\pi}^2)(\partial^\mu\boldsymbol{\pi}^2) = \frac{1}{j+1}\{\partial_\mu[(\boldsymbol{\pi}^2)^{j+1}\partial^\mu(\boldsymbol{\pi}^2)] - (\boldsymbol{\pi}^2)^{j+1}\Box\boldsymbol{\pi}^2\};
$$

$$
\partial_\mu\boldsymbol{\pi}_a\partial^\mu\boldsymbol{\pi}^a = \partial_\mu(\boldsymbol{\pi}_a\partial^\mu\boldsymbol{\pi}^a) - \frac{1}{2}\Box\boldsymbol{\pi}^2,
$$

as well as integration by parts.

From the previous expression, we see that the Feynman rules for the renormalized Lagrangian listed in Table V, as far as $\pi\pi$ scattering in the large-N limit is concerned, are equivalent to replacing

$$
(\boldsymbol{\pi}^2)^{k+1}\Box\boldsymbol{\pi}^2 \rightarrow (\boldsymbol{\pi}^2)^{k+1}G_0^{k+1}(-\Box)\Box\boldsymbol{\pi}^2. \tag{A17}
$$

Therefore, the renormalization scheme we are analyzing here is very natural in the sense that every $\boldsymbol{\pi}^2$ power in the expansion is renormalized with the same power of the G_0 function, as shown in (A17). Since those powers come from the same metric covariant function, as indicated in (A16), this is consistent with the introduction of the counterterm Lagrangians in a covariant fashion as we have discussed in Sec. III.

[1] Y. Aoki, S. Borsanyi, S. Durr, Z. Fodor, S. D. Katz, S. Krieg, and K. K. Szabo, J. High Energy Phys. 06 (2009) 088.

[2] S. Borsanyi, Z. Fodor, C. Hoelbling, S. D. Katz, S. Krieg, C. Ratti, and K. K. Szabo (Wuppertal-Budapest Collaboration), J. High Energy Phys. 09 (2010) 073.

[3] A. Bazavov, T. Bhattacharya, M. Cheng, C. DeTar, H. T. Ding, S. Gottlieb, R. Gupta, P. Hegde *et al.*, Phys. Rev. D **85**, 054503 (2012).

[4] M. I. Buchoff, M. Cheng, N. H. Christ, H.-T. Ding, C. Jung, F. Karsch, Z. Lin, and R. D. Mawhinney *et al.*, Phys. Rev. D **89**, 054514 (2014).

[5] T. Bhattacharya, M. I. Buchoff, N. H. Christ, H.-T. Ding, R. Gupta, C. Jung, F. Karsch, Z. Lin *et al.*, Phys. Rev. Lett. **113**, 082001 (2014).

[6] R. D. Pisarski and F. Wilczek, Phys. Rev. D **29**, 338 (1984).

[7] J. Berges, N. Tetradis, and C. Wetterich, Phys. Rep. **363**, 223 (2002).

[8] S. Ejiri, F. Karsch, E. Laermann, C. Miao, S. Mukherjee, P. Petreczky, C. Schmidt, W. Soeldner, and W. Unger, Phys. Rev. D **80**, 094505 (2009).

[9] T. Hatsuda and T. Kunihiro, Phys. Rev. Lett. **55**, 158 (1985).

[10] A. Bochkarev and J. I. Kapusta, Phys. Rev. D **54**, 4066 (1996).

[11] K. A. Olive *et al.* (Particle Data Group Collaboration), Chin. Phys. C **38**, 090001 (2014).

[12] J. R. Pelaez, arXiv:1510.00653.

[13] V. Bernard, U. G. Meissner, and I. Zahed, Phys. Rev. D **36**, 819 (1987).

[14] J. P. Blaizot, R. Mendez-Galain, and N. Wschebor, Ann. Phys. (Amsterdam) **307**, 209 (2003).

[15] M. Buballa, Phys. Rep. **407**, 205 (2005).

[16] S. Cortés and I. Roditi, *Local Composite Operators and the Mass Gap of the Gross-Neveu Model* (Lambert Academic Publishing, Germany, 2012).

[17] S. Weinberg, Physica A (Amsterdam) **96**, 327 (1979).

[18] J. Gasser and H. Leutwyler, Ann. Phys. (N.Y.) **158**, 142 (1984).

[19] J. Gasser and H. Leutwyler, Phys. Lett. B **184**, 83 (1987).

[20] P. Gerber and H. Leutwyler, Nucl. Phys. **B321**, 387 (1989).

[21] A. Dobado and J. R. Pelaez, Phys. Rev. D **56**, 3057 (1997).

[22] A. G. Nicola, F. J. Llanes-Estrada, and J. R. Pelaez, Phys. Lett. B **550**, 55 (2002).

[23] A. Dobado, A. G. Nicola, F. J. Llanes-Estrada, and J. R. Pelaez, Phys. Rev. C **66**, 055201 (2002).

[24] D. Fernandez-Fraile and A. G. Nicola, Eur. Phys. J. C **62**, 37 (2009).

[25] A. G. Nicola and R. T. Andres, Phys. Rev. D **89**, 116009 (2014).

[26] A. G. Nicola, J. R. de Elvira, and R. T. Andres, Phys. Rev. D **88**, 076007 (2013).

[27] A. Heinz, S. Struber, F. Giacosa, and D. H. Rischke, Phys. Rev. D **79**, 037502 (2009).

[28] A. G. Nicola, J. R. Pelaez, A. Dobado, and F. J. Llanes-Estrada, AIP Conf. Proc. **660**, 156 (2003).

[29] A. Andronic, P. Braun-Munzinger, and J. Stachel, Phys. Lett. B **673**, 142 (2009); **678**, 516(E) (2009).

[30] P. Huovinen and P. Petreczky, Nucl. Phys. **A837**, 26 (2010).

[31] R. Rapp and J. Wambach, Adv. Nucl. Phys. **25**, 1 (2002).

[32] S. Turbide, R. Rapp, and C. Gale, Phys. Rev. C **69**, 014903 (2004).

[33] A. Dobado and J. R. Pelaez, Phys. Lett. B **286**, 136 (1992).

[34] A. Dobado and J. Morales, Phys. Rev. D **52**, 2878 (1995).

[35] S. Jeon and J. I. Kapusta, Phys. Rev. D **54**, 6475 (1996).

[36] J. O. Andersen, D. Boer, and H. J. Warringa, Phys. Rev. D **70**, 116007 (2004).

[37] H. A. Weldon, Phys. Rev. D **26**, 2789 (1982).

[38] M. Le Bellac, *Thermal Field Theory* (Cambridge University Press, Cambridge, England, 1996).

[39] J. I. Kapusta and C. Gale, *Finite-Temperature Field Theory: Principles and Applications* (Cambridge University Press, Cambridge, England, 2006).

[40] J. P. Blaizot, A. Ipp, and A. Rebhan, Ann. Phys. (Amsterdam) **321**, 2128 (2006).

[41] I. S. Gerstein, R. Jackiw, S. Weinberg, and B. W. Lee, Phys. Rev. D **3**, 2486 (1971).

[42] T. Appelquist and C. W. Bernard, Phys. Rev. D **23**, 425 (1981); L. Tataru, Phys. Rev. D **12**, 3351 (1975).

[43] A. Dobado, A. Gomez-Nicola, A. L. Maroto, and J. R. Pelaez, in *Effective Lagrangians for the Standard Model*, Texts and Monographs in Physics (Springer-Verlag, New York, 1997).

[44] J. Bijnens, G. Colangelo, G. Ecker, J. Gasser, and M. E. Sainio, Phys. Lett. B **374**, 210 (1996); Nucl. Phys. **B508**, 263 (1997); **B517**, 639 (1998).

[45] J. A. Oller, E. Oset, and J. R. Pelaez, Phys. Rev. Lett. **80**, 3452 (1998).

[46] J. R. Pelaez and G. Rios, Phys. Rev. Lett. **97**, 242002 (2006).

[47] J. Zinn-Justin, *Quantum Field Theory and Critical Phenomena* (Oxford University Press, Oxford, UK, 2002).

[48] G. Leibbrandt, Rev. Mod. Phys. **47**, 849 (1975).

[49] G. Grayer *et al.*, Nucl. Phys. **B64**, 134 (1973); **B75**, 189 (1974).

[50] R. Garcia-Martin, R. Kaminski, J. R. Pelaez, and J. R. de Elvira, Phys. Rev. Lett. **107**, 072001 (2011).

[51] J. R. Batley *et al.* (NA48-2 Collaboration), Eur. Phys. J. C **70**, 635 (2010).

[52] J. Bijnens and I. Jemos, Nucl. Phys. **B854**, 631 (2012).

[53] A. G. Nicola and J. R. Pelaez, Phys. Rev. D **65**, 054009 (2002).

[54] J. Nebreda, J. R. Pelaez, and G. Rios, Phys. Rev. D **83**, 094011 (2011).

[55] A. Pelissetto and E. Vicari, Phys. Rep. **368**, 549 (2002).